



Calhoun: The NPS Institutional Archive

Theses and Dissertations

Thesis Collection

2004-09

Imaging transport: optical measurements of diffusion and drift in semiconductor materials and devices

Freeman, Will

Monterey California. Naval Postgraduate School



Calhoun is a project of the Dudley Knox Library at NPS, furthering the precepts and goals of open government and government transparency. All information contained herein has been approved for release by the NPS Public Affairs Officer.

Dudley Knox Library / Naval Postgraduate School
411 Dyer Road / 1 University Circle
Monterey, California USA 93943

<http://www.nps.edu/library>



NAVAL POSTGRADUATE SCHOOL

MONTEREY, CALIFORNIA

THESIS

**IMAGING TRANSPORT: OPTICAL
MEASUREMENTS OF DIFFUSION AND DRIFT IN
SEMICONDUCTOR MATERIALS AND DEVICES**

by

Will Freeman

September 2004

Thesis Advisor:

Nancy M. Haegel

Approved for public release; distribution is unlimited

THIS PAGE INTENTIONALLY LEFT BLANK

REPORT DOCUMENTATION PAGE			Form Approved OMB No. 0704-0188	
Public reporting burden for this collection of information is estimated to average 1 hour per response, including the time for reviewing instruction, searching existing data sources, gathering and maintaining the data needed, and completing and reviewing the collection of information. Send comments regarding this burden estimate or any other aspect of this collection of information, including suggestions for reducing this burden, to Washington headquarters Services, Directorate for Information Operations and Reports, 1215 Jefferson Davis Highway, Suite 1204, Arlington, VA 22202-4302, and to the Office of Management and Budget, Paperwork Reduction Project (0704-0188) Washington DC 20503.				
1. AGENCY USE ONLY (Leave blank)		2. REPORT DATE September 2004	3. REPORT TYPE AND DATES COVERED Master's Thesis	
4. TITLE AND SUBTITLE: Imaging Transport: Optical Measurements of Diffusion and Drift in Semiconductor Materials and Devices			5. FUNDING NUMBERS	
6. AUTHOR: Will Freeman				
7. PERFORMING ORGANIZATION NAME(S) AND ADDRESS(ES) Naval Postgraduate School Monterey, CA 93943-5000			8. PERFORMING ORGANIZATION REPORT NUMBER	
9. SPONSORING /MONITORING AGENCY NAME(S) AND ADDRESS(ES)			10. SPONSORING/MONITORING AGENCY REPORT NUMBER	
11. SUPPLEMENTARY NOTES The views expressed in this thesis are those of the author and do not reflect the official policy or position of the Department of Defense or the U.S. Government.				
12a. DISTRIBUTION / AVAILABILITY STATEMENT Approved for public release; distribution is unlimited			12b. DISTRIBUTION CODE	
13. ABSTRACT (maximum 200 words) Knowledge of transport parameters is important to the development of new optoelectronic materials and devices, such as ultraviolet (UV) semiconductor lasers and advanced solar cells. A series of experiments was performed to measure fundamental transport parameters in luminescent semiconductor materials. Using a technique that couples a scanning electron microscope (SEM) in spot mode with a charge coupled display (CCD) camera, it is possible to image the recombination of charge created at a point. The goal is to extract fundamental transport parameters, such as minority carrier diffusion length ($L_{\text{diffusion}}$) and drift length (L_{drift}), with high spatial resolution. Direct transport imaging was used to study diffusion without bias and drift under a range of applied electric fields. The recombination distribution as a function of applied bias was imaged. For the unbiased measurements, the results showed that for bulk n-type GaAs the spotwidth was independent of probe current indicating the luminescence distribution is primarily a function of generation volume and not diffusion length. For thin layer samples that could be approximated as two dimensional (2D), it was found that the spotwidth changed as a function of probe current indicating the potential to extract diffusion length data. Results are compared to numerical modeling of charge transport and the feasibility and limitations of this method for contact-free measurements of lifetime (τ) and mobility (μ) are assessed.				
14. SUBJECT TERMS Contact-less Measurements, Diffusion, Drift, Semiconductors, Transport Imaging			15. NUMBER OF PAGES 61	
			16. PRICE CODE	
17. SECURITY CLASSIFICATION OF REPORT Unclassified	18. SECURITY CLASSIFICATION OF THIS PAGE Unclassified	19. SECURITY CLASSIFICATION OF ABSTRACT Unclassified	20. LIMITATION OF ABSTRACT UL	

THIS PAGE INTENTIONALLY LEFT BLANK

Approved for public release; distribution is unlimited

**IMAGING TRANSPORT: OPTICAL MEASUREMENTS OF DIFFUSION AND
DRIFT IN SEMICONDUCTOR MATERIALS AND DEVICES**

Will Freeman
DOD Civilian, NAWCWD China Lake, California
B.S., California State University, Northridge, 1996

Submitted in partial fulfillment of the
requirements for the degree of

MASTER OF SCIENCE IN PHYSICS

**NAVAL POSTGRADUATE SCHOOL
September 2004**

Author: Will Freeman

Approved by: Professor Nancy M. Haegel
Thesis Advisor

Professor James H. Luscombe
Second Reader

Professor James H. Luscombe
Chairman, Department of Physics

THIS PAGE INTENTIONALLY LEFT BLANK

ABSTRACT

Knowledge of transport parameters is important to the development of new optoelectronic materials and devices, such as ultraviolet (UV) semiconductor lasers and advanced solar cells. A series of experiments was performed to measure fundamental transport parameters in luminescent semiconductor materials. Using a technique that couples a scanning electron microscope (SEM) in spot mode with a charge coupled display (CCD) camera, it is possible to image the recombination of charge created at a point. The goal is to extract fundamental transport parameters, such as minority carrier diffusion length ($L_{\text{diffusion}}$) and drift length (L_{drift}), with high spatial resolution. Direct transport imaging was used to study diffusion without bias and drift under a range of applied electric fields. The recombination distribution as a function of applied bias was imaged. For the unbiased measurements, the results showed that for bulk n-type GaAs the spotwidth was independent of probe current indicating the luminescence distribution is primarily a function of generation volume and not diffusion length. For thin layer samples that could be approximated as two dimensional (2D), it was found that the spotwidth changed as a function of probe current indicating the potential to extract diffusion length data. Results are compared to numerical modeling of charge transport and the feasibility and limitations of this method for contact-free measurements of lifetime (τ) and mobility (μ) are assessed.

THIS PAGE INTENTIONALLY LEFT BLANK

TABLE OF CONTENTS

I.	INTRODUCTION.....	1
A.	TRANSPORT IN SEMICONDUCTORS.....	1
B.	PURPOSE OF THESIS.....	1
C.	MILITARY RELEVANCE.....	2
D.	THESIS OVERVIEW	2
II.	TRANSPORT PARAMETERS.....	3
A.	DIFFUSION AND DRIFT	3
B.	LUMINECSCENCE IN SEMICONDUCTORS.....	6
III.	IMAGING TRANSPORT	11
A.	DIRECT TRANSPORT IMAGING	11
B.	DRIFT MEASUREMENTS.....	13
C.	DIFFUSION MEASUREMENTS	19
1.	Bulk GaAs.....	19
2.	Epitaxial AlGaAs	23
3.	GaAs/GaNAs Quantum Well.....	27
a.	<i>Panchromatic</i>	28
b.	<i>950 nm Long Pass Filter, GaNAs Layer</i> <i>Luminescence.....</i>	32
c.	<i>950 nm Short Pass Filter, GaAs Layer</i> <i>Luminescence.....</i>	35
D.	COMPARISON TO COMPUTER MODEL	40
IV.	CONCLUSIONS	43
	LIST OF REFERENCES.....	45
	INITIAL DISTRIBUTION LIST	47

THIS PAGE INTENTIONALLY LEFT BLANK

LIST OF FIGURES

Fig. 1.	Excess Minority Carrier Distribution as a Function of Distance from Generation Point	10
Fig. 2.	SEM and CCD Camera	11
Fig. 3.	Images of Bulk n-Type GaAs	12
Fig. 4.	Sample 329SI Contacts	13
Fig. 5.	Charge Motion Under Applied Bias	15
Fig. 6.	Charge Motion Under Applied Bias, Subtracted	17
Fig. 7.	Bulk GaAs, Luminescent Spot, Raw Data and Spline Interpolated Data	20
Fig. 8.	Bulk GaAs, Luminescent Spot for Accelerating Voltages 15 to 35 kV	21
Fig. 9.	Bulk GaAs, Spotwidth as a Function of Accelerating Voltage	21
Fig. 10.	Bulk GaAs, Luminescent Spot for Probe Currents 1×10^{-10} to 1×10^{-7} A	22
Fig. 11.	Bulk GaAs, Spotwidth as a Function of Probe Current	22
Fig. 12.	Excitation Volume, 2D and 3D Sample	24
Fig. 13.	1 μ m AlGaAs, Luminescent Spot for Probe Currents 1×10^{-10} to 1×10^{-7} A	25
Fig. 14.	1 μ m AlGaAs, Spotwidth as a Function of Probe Current	25
Fig. 15.	1 μ m AlGaAs and Bulk GaAs, Spotwidth as a Function of Probe Current	26
Fig. 16.	GaAs/GaNAs, Panchromatic, Raw Data, Luminescent Spot for Probe Current 1×10^{-7} A	29
Fig. 17.	GaAs/GaNAs, Panchromatic, Spline Data, Luminescent Spot for Probe Current 1×10^{-7} A	29
Fig. 18.	GaAs/GaNAs, Sample n554a, Panchromatic, Spotwidth vs Spatial Samples	30
Fig. 19.	GaAs/GaNAs, Sample n546, Panchromatic, Spotwidth vs Spatial Samples	30
Fig. 20.	GaAs/GaNAs, Sample n553, Panchromatic, Spotwidth vs Spatial Samples	31
Fig. 21.	GaAs/GaNAs, LPF GaNAs Luminescence, Raw Data, Luminescent Spot for Probe Current 1×10^{-7} A	33
Fig. 22.	GaAs/GaNAs, LPF GaNAs Luminescence, Spline Data, Luminescent Spot for Probe Current 1×10^{-7} A	33
Fig. 23.	GaAs/GaNAs, Sample n554a, LPF GaNAs Luminescence, Spotwidth vs Spatial Samples	34
Fig. 24.	GaAs/GaNAs, Sample n546, LPF GaNAs Luminescence, Spotwidth vs Spatial Samples	34
Fig. 25.	GaAs/GaNAs, Sample n553, LPF GaNAs Luminescence, Spotwidth vs Spatial Samples	35

Fig. 26.	GaAs/GaNAs, SPF GaAs Luminescence, Raw Data, Luminescent Spot for Probe Current 1×10^{-7} A	37
Fig. 27.	GaAs/GaNAs, SPF GaAs Luminescence, Spline Data, Luminescent Spot for Probe Current 1×10^{-7} A	37
Fig. 28.	GaAs/GaNAs, Sample n554a, SPF GaAs Luminescence, Spotwidth vs Spatial Samples	38
Fig. 29.	GaAs/GaNAs, Sample n546, SPF GaAs Luminescence, Spotwidth vs Spatial Samples	38
Fig. 30.	GaAs/GaNAs, Sample n553, SPF GaAs Luminescence, Spotwidth vs Spatial Samples	39
Fig. 31.	Computer Modeled and Measured Charge Motion Under Applied Bias, Subtracted	42
Fig. 32.	Computer Modeled Spot for Mobility Lifetime Products 1.6×10^{-6} , 1.8×10^{-6} , and 3.48×10^{-6} cm^2/V	42

ACKNOWLEDGMENTS

I would like to thank Professor Nancy Haegel for her help and for creating a great academic environment within the laboratory to work in. The work presented in this paper stemmed from many of her suggestions and leveraged off of her previous original work.

I would also like to thank Ben Cardozo at Lawrence Berkeley National Laboratory for the GaAs samples and Homan Yuen at Stanford University for the QW samples.

THIS PAGE INTENTIONALLY LEFT BLANK

I. INTRODUCTION

A. TRANSPORT IN SEMICONDUCTORS

Semiconductor technology is important in the development of advanced solid state devices for electronics and optoelectronics. Semiconductors are used in ultraviolet (UV) semiconductor lasers, solar cells, infrared (IR) detectors, and many other electronic devices. Many IR and radar detectors/devices use semiconductor technology. Semiconductors are unique in their ability to detect and produce photons across a wide range of the electromagnetic spectrum.

Imaging charge carrier motion in semiconductors allows localized spatial variation to be examined. The technique used in this analysis, charge transport imaging, was introduced in 2003 and combines the spatial resolution of a scanning electron microscope (SEM) with the optical imaging provided by a charge coupled display (CCD) camera [1]. This technique allows monitoring of charge transport in luminescent semiconductor materials while maintaining spatial imaging of the recombination process. Keeping the charge generation at a fixed location (point), observation of diffusion and drift by imaging the luminescence from the recombination is possible. The key differences between this and cathodoluminescence (CL) is that the spatial resolution from the recombination is maintained. This has the advantage for cases in which the diffusion or drift of charge produces luminescence at locations away from the generation point.

In this work, drift behavior has been directly imaged in high purity epitaxial GaAs under an applied bias. The technique has also been used to image the diffusive motion of charge in epitaxial layers of n-type GaAs and other semiconductor materials. Experimental data and simulated computer model generated results are compared. Feasibility into using such techniques for contact-free measurements is also discussed.

B. PURPOSE OF THIS THESIS

The purpose of this paper is to examine drift and diffusion in luminescent semiconductors. This will be done for bulk materials which are characterized as three dimensional (3D) and for thin epitaxial materials that can be approximated as two

dimensional (2D). These measurements were performed using a new experimental technique called direct transport imaging. This was done utilizing a SEM coupled with a thermoelectrically cooled CCD camera in the Physics Department at the Naval Postgraduate School (NPS). A series of experiments was performed to measure fundamental transport parameters in semiconductor materials. The goal was to extract fundamental transport parameters with high spatial resolution. The feasibility and limitations of this method for contact-free measurements are assessed.

C. MILITARY RELEVANCE

Transport parameters are important to the development of new optoelectronic materials and devices. Devices such as UV semiconductor lasers and advanced solar cells for example are just some of the devices that could benefit from such a study. The ability to image charge transport could potentially lead to being able to measure the effects of defects on charge transport in semiconductor devices. Potential cost savings could also be achieved by enabling transport characterization with minimal or no additional contact processing. This could speed the development of new materials and reduce technology transfer time for new semiconductor technologies.

D. THESIS OVERVIEW

Chapter I describes an overview of the direct transport imaging technique and describes the importance to military semiconductor devices. The need to image transport in luminescent semiconductor devices leads to the investigation of diffusion and drift in semiconductors, the main objective of this thesis. Fundamental concepts of charge transport parameters are described in Chapter II. Chapter III discusses imaging transport with and without an applied bias and comparisons are made to computer modeling. Conclusions are discussed in Chapter IV.

II. TRANSPORT PARAMETERS

A. DIFFUSION AND DRIFT

Semiconductor materials are characterized by a bandgap of forbidden states, separating a filled valence band (VB) from an empty conduction band of available electron states. At temperatures above absolute zero, electrons are thermally excited from the VB and generate electron-hole pairs. The average intrinsic carrier concentration (n_i) is constant for a given temperature. In parallel, some recombination will bring the electrons from the conduction band (CB) to the VB. In direct bandgap semiconductors, recombination yields emission of a photon. In indirect bandgap semiconductors, a majority of recombination takes place through intermediate states by means of phonon emission.

If this equilibrium is disturbed by an external excitation source, such as an incident electron beam or from incident photons, additional carriers will be created. Let n_{no} and p_{no} denote the electron and hole concentrations in the absence of excitation and n_n and p_n denote the electron and hole concentrations with excitation (concentrations are per volume). If the sample is n-type, the majority carriers are the electrons and the minority carriers are the holes. Likewise, if the sample is p-type, the majority carriers are the holes and the minority carriers are the electrons. For illustrative purposes, consider the n-type case. Without excitation, it is known

$$n_{no} p_{no} = n_i^2 \quad (1)$$

When excitation is present, equal number of electron-hole pairs will be created and of course the product np will not equal n_i^2 . However, the following two differences will be equal [2]

$$\Delta n_n = n_n - n_{no} = p_n - p_{no} = \Delta p_n \quad (2)$$

Since the material being considered is n-type, $n_{no} \sim N_d$, and p_{no} is found to be much less from Equation 1. If the Δn_n changes by a small percentage, the Δp_n will of course change drastically. Therefore, the minority carriers change drastically while the majority carriers do not change much (percentage wise). Thus, the electrical properties under excitation are often determined by the minority carriers.

Diffusion is the motion of carriers due to a concentration gradient, for example formed by photogeneration or other excitation. Drift on the other hand, is the motion of carriers due to an applied bias. Currents in semiconductor devices are the result of both diffusion and drift currents.

The diffusion length ($L_{\text{diffusion}}$), which is the length a carrier will travel before it recombines, can be found from the well known equation

$$L_{\text{diffusion}} = \sqrt{D\tau} \quad (3)$$

where τ is the mean free time (or lifetime as used in this context) and D is the diffusion coefficient. The diffusion coefficient is found from the Einstein relation

$$D = kT\mu/e \quad (4)$$

where k is Boltzmann's constant, T is the temperature, and μ is the mobility. There is a diffusion coefficient for electrons and holes. They differ in part by the mobility ($\mu = e\tau/m^*$) for the electrons and holes respectively (μ_e, μ_h), where m^* is the effective mass of either the electron or hole [3]. The constant e is the usual electron charge.

The drift length (L_{drift}), which is the average length a carrier will travel due to an applied electric field (E), can be expressed as

$$L_{\text{drift}} = \mu E \tau \quad (5)$$

The mobility (μ) appearing in the above equations is the constant of proportionality between the drift velocity (v_{drift}) and the applied electric field. This can be expressed mathematically simply as

$$v_{\text{drift}} = \mu E \quad (6)$$

In general, the total current in a semiconductor material can be expressed as $J = J_{\text{drift}} + J_{\text{diffusion}} + J_{\text{displacement}}$ (for both electrons and holes). At steady state, the displacement term is zero and the current due to the electrons and holes is

$$J_e = en\mu_e E + eD_e dn/dx \quad (7)$$

$$J_h = en\mu_h E + eD_h dp/dx$$

The minority carrier lifetime is generally measured by what is known as the photoconduction effect. The equation for this effect is [4]

$$J_{\text{pc}} = e(\mu_e + \mu_h)\Delta n E \quad (8)$$

where J_{pc} is the incremental current density as a result of the illumination, Δn is the number of electron-hole pairs per volume created by the illumination and the other symbols have the usual meaning. Since $\Delta n = \tau G$ resulting from photon generation rate (G), the lifetime is given by [4]

$$\tau = J_{pc} / [G E e (\mu_e + \mu_h)] \sim J_{pc} \quad (9)$$

This technique, however, requires precise knowledge of the generation rate, which can be a complex combination of optical source, sample surface, absorption, and system optics.

Another standard technique of measuring minority carrier lifetime is using the Stevenson-Keyes method [5]. The experimental set-up consists of a bias applied to a sample with contacts and illuminated by a light pulse. An oscilloscope is connected at one end which represents the load resistance. Solution to the differential equation for the transport with appropriate boundary conditions is [4]

$$p_n(t) = p_{no} + \tau_h G \exp(-t/\tau_h) \quad (10)$$

The decay is measured by the oscilloscope and this allows for determination of the lifetime. Time resolved luminescence can also measure minority carrier lifetime. This requires pulsed lasers and fast detectors that can match the wide range (approximately 10^{-3} to 10^{-12} sec) of observed lifetimes in semiconductor materials. This is an established and widely used approach. However, it does not provide the complementary information on mobility that is needed for diffusion or drift lengths, which depend on the $\mu\tau$ product.

One standard technique of measuring minority carrier drift mobility is that of Haynes-Shockley [6]. Basically, localized light pulses are used to generate carriers in the sample. Solution to the transport equation with appropriate boundary conditions with an applied electric field yields [4]

$$p_n(x, t) = \frac{N}{\sqrt{4\pi D_h \tau}} \exp[-(x - \mu_h E t)^2 / (4 D_h t) - t/\tau_h] + p_{no} \quad (11)$$

Again, an oscilloscope is used. By knowing the sample length, applied electric field, and the time delay from the applied field and detected pulse (from the oscilloscope), the drift mobility $\mu = x/(Et)$ can be determined.

A disadvantage of many of the standard methods described is that the sample must have contacts. Spatial uniformity is also assumed over the length of the sample.

This thesis will discuss a potential alternative approach that could lead the way for a technique that does not require contacts on the sample and can provide spatial resolution on the micron scale.

B. LUMINESCENCE IN SEMICONDUCTORS

Luminescence is the emission of light, in excess of thermal radiation, caused by external source excitation. There are several types of external excitation that can cause luminescence. In photon-excitation, the source is in the form of photons (electromagnetic radiation). An example of photo-excitation would be the photoluminescence (PL) technique. Another type of external excitation is electron beam excitation in which an energetic electron beam is used to bombard the sample to create luminescence. This is the type of source excitation that is used in the direct transport imaging technique addressed in this work. It is also commonly used in more conventional techniques such as CL. There are other types of excitation, such as chemiluminescence and electroluminescence, which are not pertinent to the discussion here [7].

When the incident electron or photon energy is greater than the bandgap, this often leads in semiconductor materials to electron-hole pair production. When these carriers recombine, light is produced at wavelengths corresponding to the allowed energy states of the material (intrinsic, extrinsic) ($\Delta E = 1.24/\lambda$, where energy E is in eV and the wavelength is in μm). This process is most efficient in direct bandgap materials.

In the case of electron beam excitation, many electron-hole pairs are created through different mechanisms such as backscatter electrons, primary and secondary electrons. Electron beam excitation is capable of producing many orders of magnitude greater carrier generation than photo-excitation. This is one of the advantages to electron beam excitation that can be useful in wide bandgap materials. There are two types of scattering mechanisms, elastic and inelastic. Rutherford scattering of electrons by the nuclei of atoms is an example of elastic scattering. Elastic scattering of electrons gives rise to high energy backscattered electrons in the SEM [7]. Inelastic scattering may include secondary electron emission, electron-hole pair generation, x-rays, and thermal

effects to name a few. Inelastic interaction processes are useful in electron probe instruments.

When an electron beam is incident on a material, the electrons undergo a series of successive elastic and inelastic scattering events. One result of this is the original trajectories of the electrons are altered in a random fashion. Monte Carlo trajectory simulation is one method of predicting the electron beam energy dissipation in solids, i.e., the generation volume and penetration depth. It is difficult to model the scattering path though in a solid [7].

There are several statistical model expressions to estimate the electron penetration depth. One general expression derived by Kanaya and Okayama has been found to agree well with experimental results over a wide range of atomic numbers [8]. The penetration depth estimate in μm is

$$R_e = [0.0276A/(\rho Z^{0.889})]E_b^{1.67} \quad (12)$$

where E_b is in keV, A is the atomic molecular mass (g/mol), ρ is in g/cm^3 , and Z is the atomic number. As an example, consider the case of bulk GaAs. At 35 keV electron beam energy, the estimated penetration depth is approximately 6 μm . At 20 keV the penetration depth is slightly over 2 μm while at 10 keV it is estimated to be slightly below 1 μm . Other models such as the Everhart-Hoff expression [9] estimate somewhat lower penetration depths. Nevertheless, all these expressions are useful in light of the fact they give approximate penetration depths.

Electron beam excitation has the advantage of being able to control to a certain degree the penetration depth into the sample material by varying the accelerating voltage of the electron beam. In comparison to PL, where most of the incident photons are absorbed very close to the surface and thus limit the depth of light penetration and excitation volume, electron beam excitation can achieve much greater depth penetration as discussed from the statistical simulation findings. As an example of PL penetration depths, consider green light ($\lambda = 514 \text{ nm}$) incident on GaAs. Most photons are absorbed within the first 0.77 μm of the surface [10]. It is further noted that typically thousands of electron-hole pairs are generated by a 20 keV electron while one photon generates only one electron-hole pair in PL.

The carrier generation distribution, or just generation volume, is naturally of interest in the study of electron beam excitation. A number of approximations for the generation distribution have been used such as point source, sphere, and Gaussian. The Gaussian models of the type

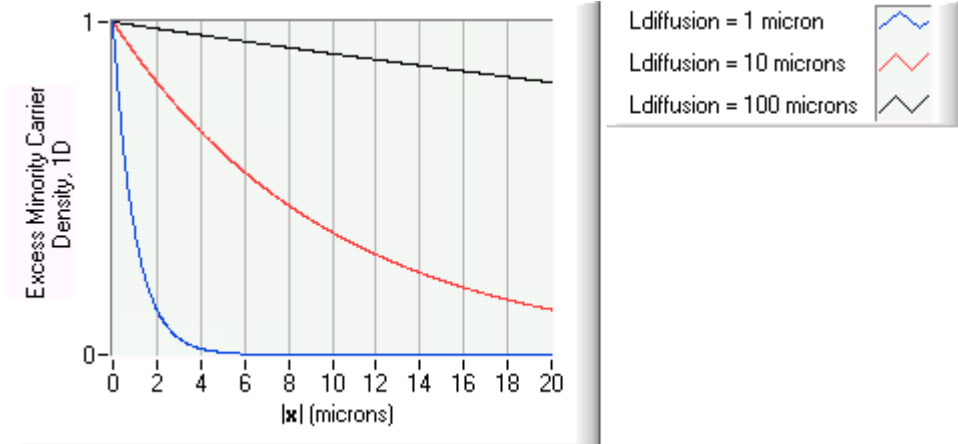
$$F(z) = F_0 \exp[-a^2(z - z_0)^2] \quad (13)$$

have been shown to provide accurate estimates [7]. Comparison to Monte Carlo calculations [7] show that the generation volume is not perfectly defined. However, contours of equal energy dissipation are in good agreement and indicate that most of the energy is dissipated in a small volume near the electron beam impact point. The excess minority carrier density is different for the one dimensional (1D), 2D and three 3D cases. In the 1D case the excess minority carrier density decreases as $\sim \exp(-|x|/L_{\text{diffusion}})$ [11]. In the 2D case the density decreases as $\sim K_0(|x|/L_{\text{diffusion}})$ [1], where K_0 is a zero order modified Bessel function of the second kind, while in the 3D case the density decreases as $\sim 1/|x| \exp(-|x|/L_{\text{diffusion}})$ [11]. Shown in Figure 1 is how the normalized excess minority carrier density changes as a function of distance for the 1D, 2D, and 3D cases assuming a point generation (with diffusion lengths of 1, 10, and 100 μm). It is readily seen that the excess minority carrier density for the 3D case drops off rapidly. However, for the 2D and 1D cases the excess minority carrier density does not drop off as rapidly.

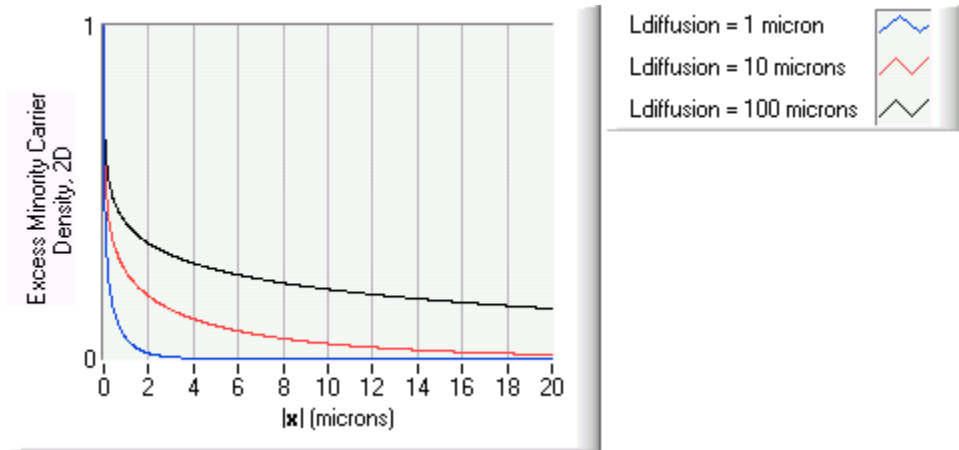
This is important in transport imaging because these are parameters that affect the imaged spotwidth. This allows understanding of the relation between carrier generation and the region of luminescent recombination. We consider the effect of diffusion from a point. The 3D case spot diameter is seen to be basically independent of $L_{\text{diffusion}}$ and therefore primarily dependent on the generation volume. Donolato has shown that this fact is what allows the resolution of CL defect imaging to be unaffected by carrier diffusion [11]. However, the 2D case spot diameter is seen to reflect the carrier diffusion length for diffusion lengths greater than the generation volume.

It should be expected for bulk materials that are definitely 3D, variation in the spotwidth should not change much as a function of diffusion length. For thin sample materials that can be approximated as 2D (or samples that can be approximated as 1D),

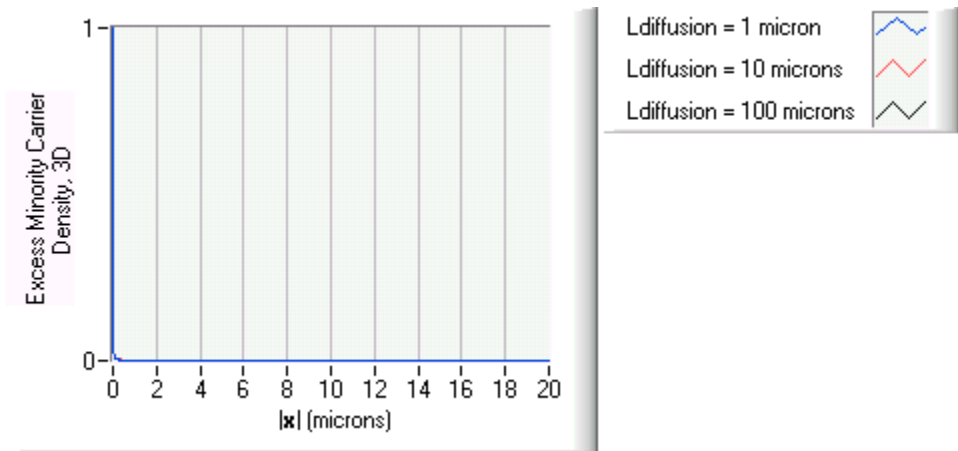
the spotwidth should change as a function of diffusion length. One experimental goal of this work is to confirm this prediction.



(a) 1D.



(b) 2D.



(c) 3D.

FIGURE 1. Excess Minority Carrier Distribution as a Function of Distance from Generation Point.

III. IMAGING TRANSPORT

A. DIRECT TRANSPORT IMAGING

Direct transport imaging is a relatively new technique that combines the charge generation capability of a SEM, the resolution of an optical microscope, and the sensitivity of a CCD camera [1]. The CCD is used to capture the luminescence of a sample under electron beam excitation. This technique preserves the spatial information of the charge recombination. This is the primary difference of the technique compared to conventional CL. The electron beam in the SEM is used in spot mode to generate free carriers in the sample. When the carriers recombine, the luminescence is captured by the CCD camera.

The current system utilizes a JEOL 840A SEM. An optical microscope is inserted into the chamber and connects externally to the thermoelectrically cooled Apogee CCD camera. Shown in Figure 2 is the SEM and CCD camera experimental set-up. The silicon detector in the CCD camera covers the band from approximately 400 to 1,100 nm. Any unfiltered image would include all wavelengths within this band. The resolution of this system is approximately $0.4\text{ }\mu\text{m/pixel}$. The CCD is cooled to -15°C to minimize thermal noise. The system consists of a mirror with a hole for the electron beam to pass through. An optical microscope at the end of the apparatus magnifies and focuses the luminescence from the sample onto the focal plane of the CCD array.



FIGURE 2. SEM and CCD Camera.

The SEM can collect data in either picture (pic) mode or spot mode (as well as other modes not pertinent to the discussion here). In pic mode, the electron beam is raster scanned across the sample. The luminescence is recorded by the CCD. This mode differs from CL in that the camera exposure time can be much longer than a single frame in CL. Traditional CL imagery uses a continuously scanned beam. In spot mode, the electron beam of the SEM is held at a fixed location (point). The generation point can be precisely controlled which allows for the local charge diffusion to be recorded. This can be done with or without an external bias to study the mobility and drift of the minority carriers.

As an example, consider the case of bulk n-type GaAs doped at $n = 5.9 \times 10^{17} \text{ cm}^{-3}$. Shown in Figure 3 is the resulting image from the CCD in both pic mode and spot mode for this sample. No applied bias is introduced. The probe current was set at $6 \times 10^{-10} \text{ A}$, the accelerating voltage was 35 kV, and the shutter exposure on the CCD camera was set at 1 sec. The images are 512 by 512 pixels, and since each pixel corresponds to approximately $0.4 \text{ } \mu\text{m}$ at the sample, the resulting image size is approximately 205 by 205 μm .

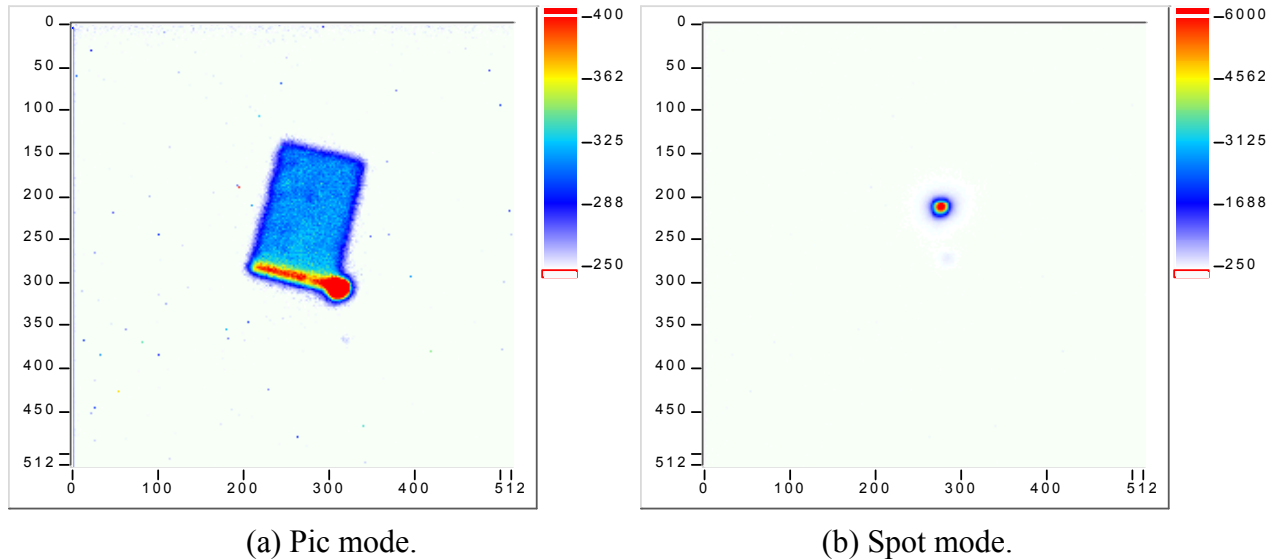


FIGURE 3. Images of Bulk n-Type GaAs.

In Figure 3a, the area with the brightest intensity is the region over which the electron beam was scanned. From the figure it is apparent at the area scanned in pic mode by the SEM at this magnification (2000 X) is less than the area that which captured by the CCD. The high intensity strip on the lower edge is a result of the SEM always scanning the

beam longer on one of the raster scan edges. In Figure 3b the light generated by the electron beam at a fixed point is seen. It should be noted that the intensity scales on the two figures are not the same, with the spot mode picture range being higher because of the increased intensity focused at one location (point).

B. DRIFT MEASUREMENTS

Using the direct transport imaging technique, measurements were made while applying an external bias in order to image the drift motion of the minority carriers. The sample (329SI) was n-type GaAs obtained from Lawrence Berkeley National Laboratory. This sample was a high purity epitaxial layer doped at $N_D - N_A = 5.1 \times 10^{13} \text{ cm}^{-3}$. The layer thickness was approximately 60 to 80 μm on top of a semi-insulating GaAs substrate. The sample had ion implanted contacts. The Au/Ge contacting metal layers were evaporated on the top of the sample spaced approximately 2 mm apart. Shown in Figure 4 is a schematic top view of the sample and contact geometry.

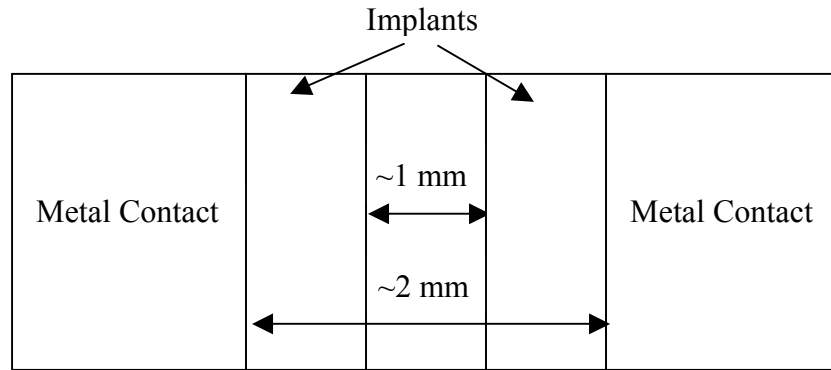


FIGURE 4. Sample 329SI Contacts.

The implanted contacts spacing, though not visible, was approximately 1 mm. The SEM accelerating voltage was set at 35 kV and the probe current at $3 \times 10^{-8} \text{ A}$. The bias was varied from +100 to -100 V. Thus, the highest applied electric field was approximately 100 V/mm. Shown in Figure 5 are images of the recombination distribution as a function of applied bias. Notice that in the zero bias image (0 V) the spot is present without any drift as expected. The drift of the charge is readily seen from the images captured by the CCD. Since the material is n-type, the motion of holes is being imaged, i.e., the holes are

the minority carriers which are recombining to produce the illumination. The images are 512 by 1024 pixels which corresponds to approximately 205 by 410 μm . Comparison of the 100 V image to the 0 V image reveals a long extended tail approximately 120 μm in the figure imaging the charge carrier motion. For intermediate applied voltages between ± 100 V and 0 V, the tail becomes less extended and broadens as the applied voltage decreases as expected. The small circular spot next to the electron beam generated spot, most noticeable in the zero bias case, is believed to be a result from a small reflection within the system.

In the measurements discussed and shown in Figure 5, all the drift images include the direct spot from the electron beam. In order to isolate and image the field induced charge motion, the direct spot at zero bias was subtracted from the images taken at the other biases. Shown in Figure 6 are images of the recombination distribution as a function of applied bias with the direct spot subtracted. These are the same images as in Figure 5 except that now the images have been subtracted. Notice in the 0 V image only the mostly white background, corresponding to the noise background, is present. This is as expected since the direct spot has been subtracted.

Other samples were measured besides the one shown in Figures 5 and 6. All experimentally recorded measurements to date have shown a similar trend as illustrated here for luminescent semiconductor materials. The results shown are characteristic of such materials. Comparison of different materials using this approach could be used to measure drift length and the material parameters ($\mu\tau$) that determine it. Also, measurement of the local field can check for field uniformity and/or voltage drop at contacts.

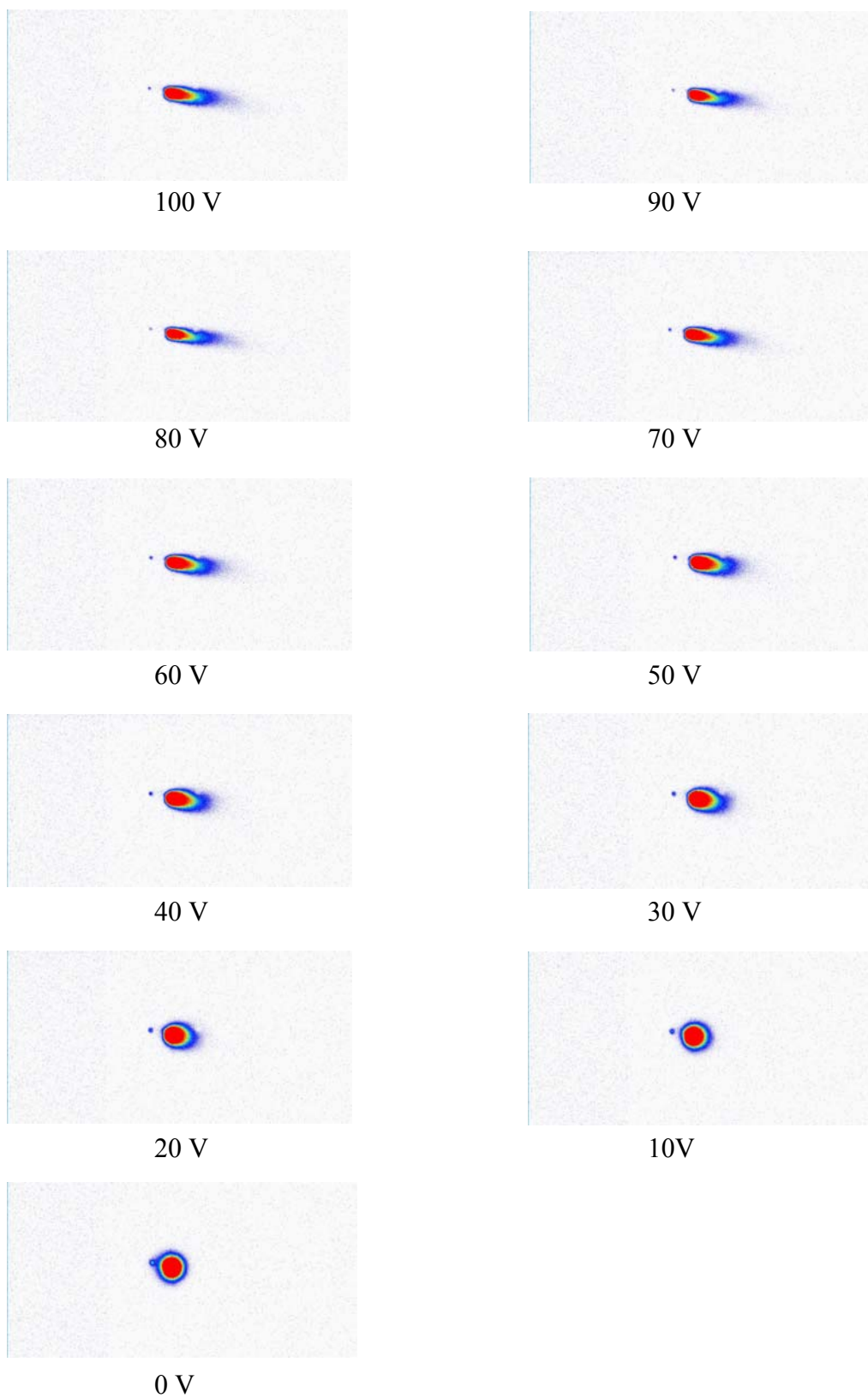
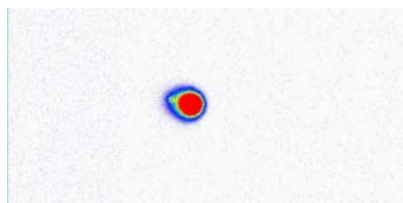
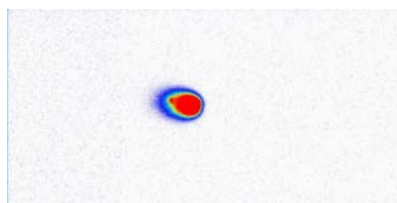


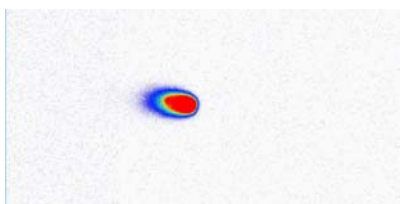
FIGURE 5. Charge Motion Under Applied Bias.



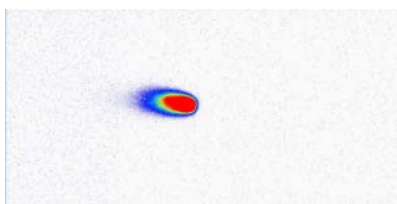
-10V



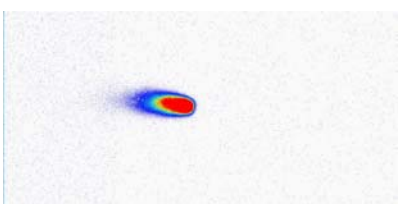
-20V



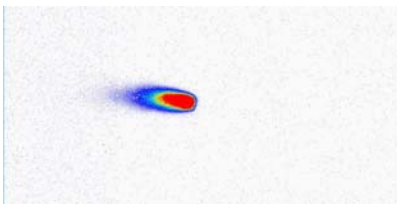
-30 V



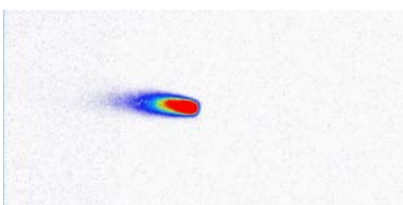
-40 V



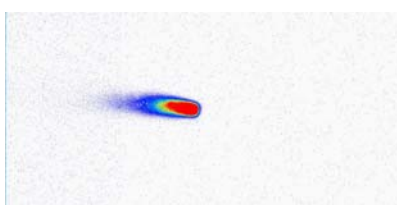
-50 V



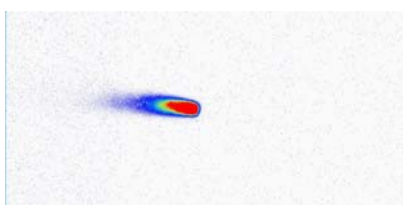
-60 V



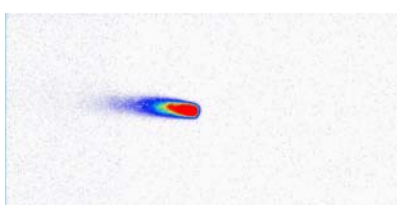
-70 V



-80 V



-90 V



-100 V

FIGURE 5. (Contd.)

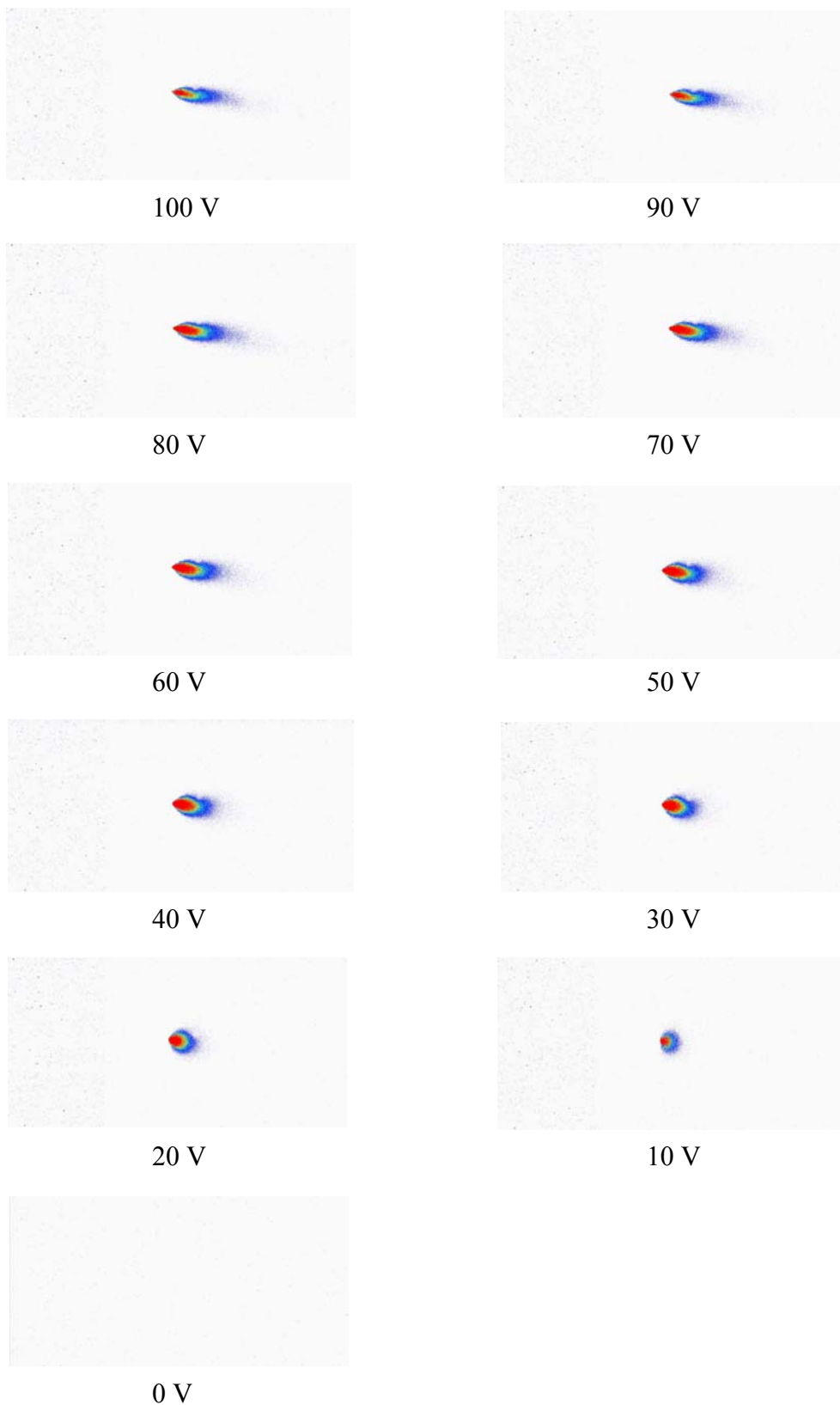
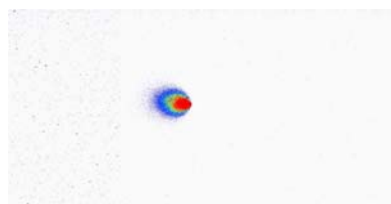


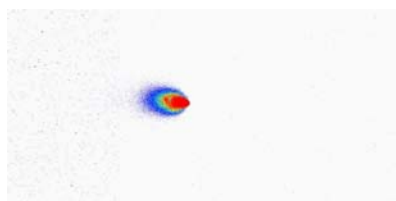
FIGURE 6. Charge Motion Under Applied Bias, Subtracted.



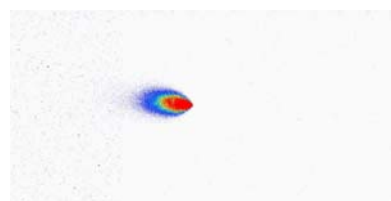
-10 V



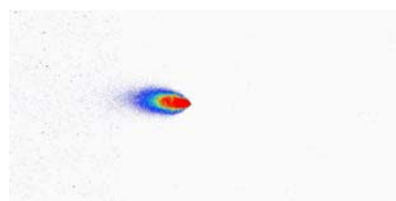
-20 V



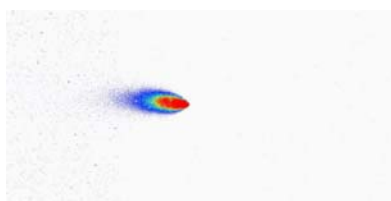
-30 V



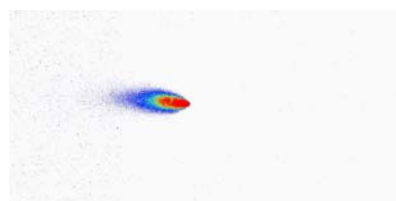
-40 V



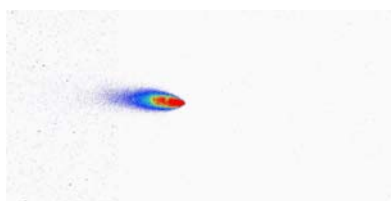
-50 V



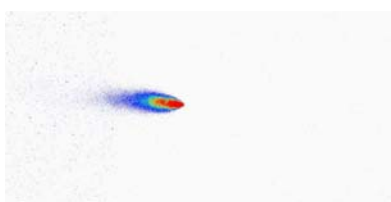
-60 V



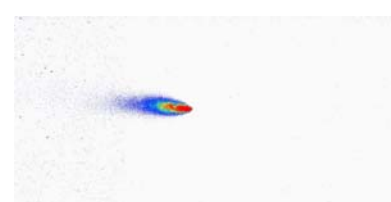
-70 V



-80 V



-90 V



-100 V

FIGURE 6. (Contd.)

C. DIFFUSION MEASUREMENTS

1. Bulk GaAs

Using the transport imaging technique, measurements were made on bulk n-type GaAs sample doped at $n = 5.9 \times 10^{17} \text{ cm}^{-3}$ without applying any external bias in order to image the spotwidth under conditions of purely diffusive transport. The first set of measurements made was the spotwidth as a function of electron accelerating voltage. Since the differences in spotwidth between incremental accelerating voltages was on the order of the resolution of the current optics in the system (approximately $0.4 \text{ } \mu\text{m}/\text{pixel}$), a spline interpolation was used [12]. Shown in Figure 7 is the raw data and the spline interpolated data at 30 kV. It is seen that the spline accurately interpolates the data without distorting the raw data points. Spline interpolation was used on all data that follows. The accelerating voltage was varied from 15 to 35 kV. Shown in Figure 8 are the spots for various accelerating voltages. Since the background pixels are nonzero, the spots are normalized so that the calculated half power spotwidths (referred to simply as spotwidth in this paper) will be correct. The 2D images were recorded and 1D cuts through the spots are shown in the figure. The x axis of the graph is displayed in units of pixels with the center pixel being set to zero for ease of seeing the spotwidths. Figure 9 shows the measured spotwidth as a function of accelerating voltage. It is noted that the spotwidth increases as a function of accelerating voltage. This is as expected since the accelerating voltage is increasing the penetration depth of the electron beam and thus increasing the generation volume of the minority free carriers. As discussed in a previous section, we expect the generation volume to determine the luminescence spotwidth in the thick sample limit.

Next the spotwidth was measured as a function of probe current. The accelerating voltage was kept constant at 30 kV. Shown in Figure 10 are the 1D cuts of the spot for probe currents varied from 1×10^{-10} to 1×10^{-7} A. Shown in Figure 11 is the spotwidth as a function of probe current. It is seen from these graphs that the spotwidth does not change and is basically constant in the bulk sample when the probe current is varied. The average or mean was found to be 10.11 pixels with a standard deviation of 0.17 pixels. This is in agreement with Donolato's results. Since the sample is definitely 3D, we expect that the

generation volume should not change much as the probe current changes because the generated spot size is less than the excitation volume diameter. For example, a probe current of 6×10^{-12} A has a beam radius of approximately 5 nm, which is much less than the generation volume radius. This corresponds to an area of 7.85×10^{-17} m². As the probe current is increased to 1×10^{-7} A, the area is increased to approximately 1.3×10^{-12} m² which corresponds to a radius of approximately 645.5 nm or 0.646 μ m (or perhaps somewhat greater). This is still less than the penetration depth and generation radius at 30 kV.

Because of the large range of probe currents and accelerating voltages used in these measurements, it is often desirable to vary the shutter time. Measurements of the spotwidth as a function of shutter time on the CCD were made. The accelerating voltage was held constant at 30 kV, the probe current was held constant at 3×10^{-9} A, and the exposure time was varied. It was found that changing the exposure time did not affect the normalized spotwidth measurements as long as the pixels were not saturated and it was not noisy. If the exposure time was increased so that the center of the spot saturated the pixels, the data of course was not useable. Thus, as long as the CCD is not saturated, varying the exposure time did not affect the spotwidth measurements.

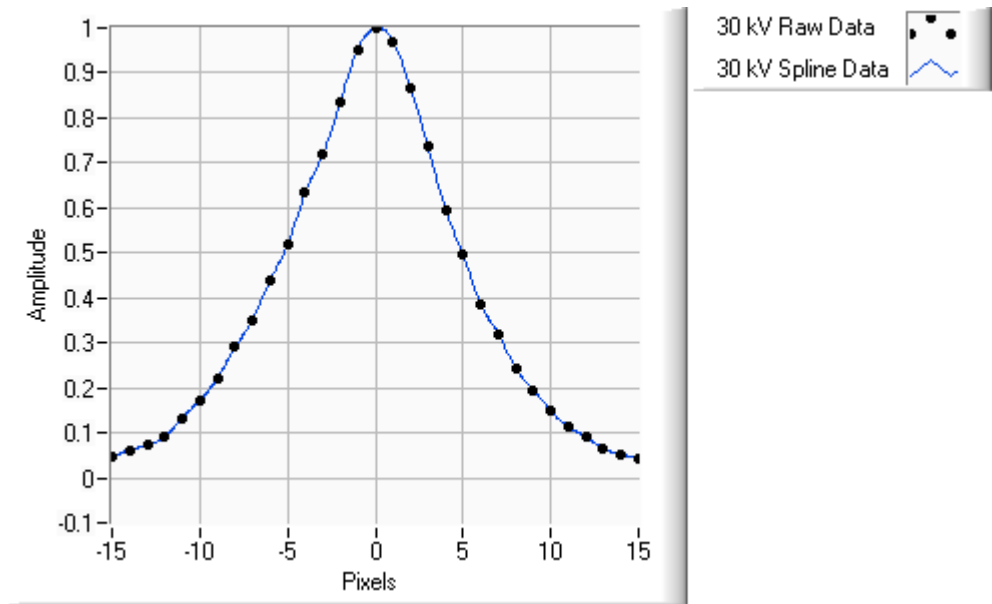


FIGURE 7. Bulk GaAs,
Luminescent Spot, Raw Data and Spline Interpolated Data.

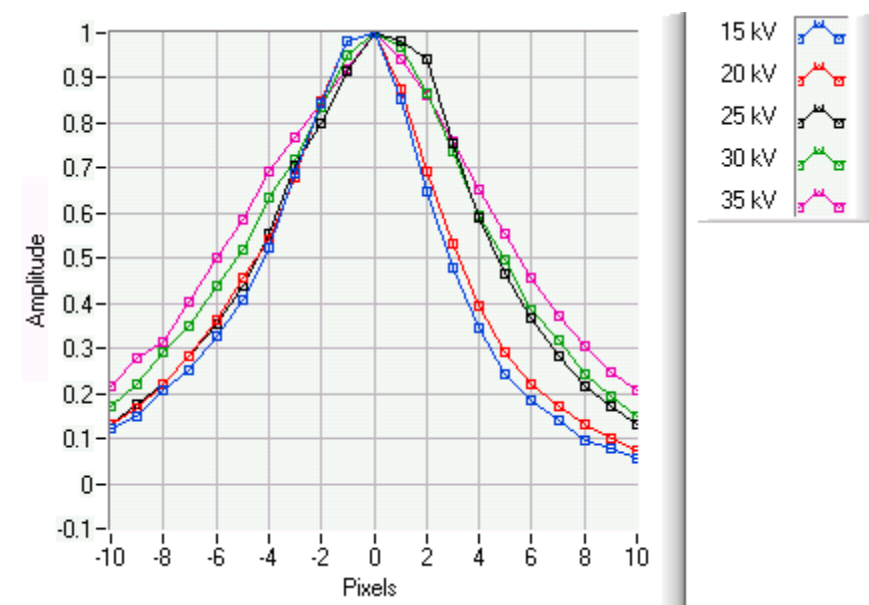


FIGURE 8. Bulk GaAs,
Luminescent Spot for Accelerating Voltages 15 to 35 kV.

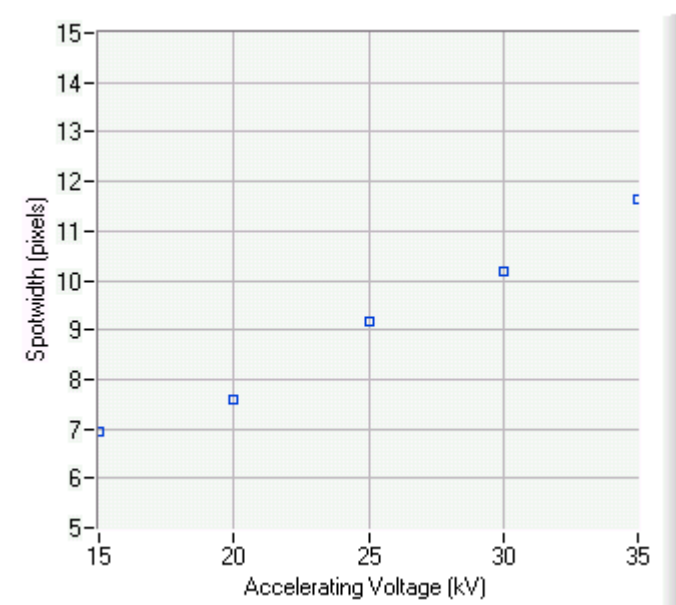


FIGURE 9. Bulk GaAs,
Spotwidth as a Function of Accelerating Voltage.

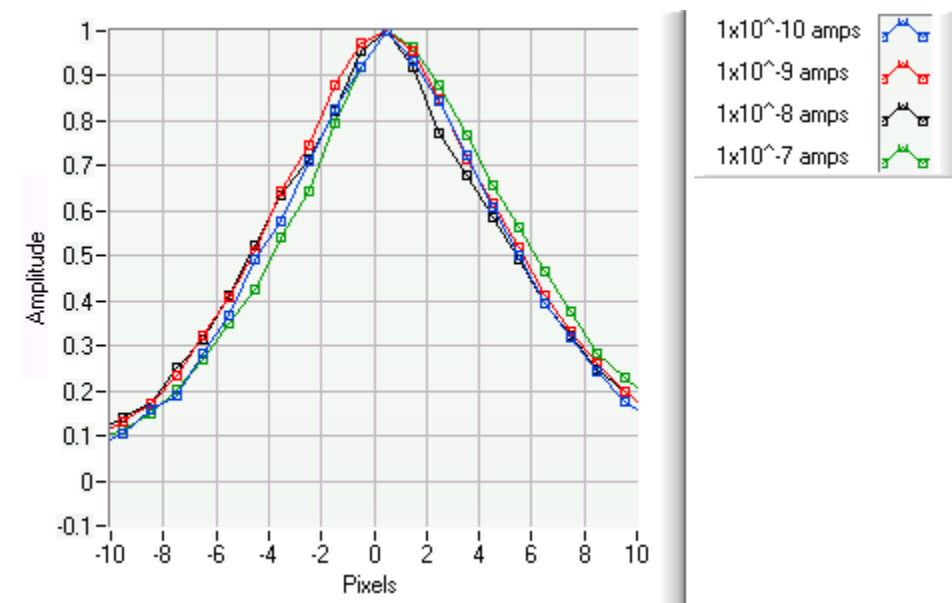


FIGURE 10. Bulk GaAs,
Luminescent Spot for Probe Currents 1×10^{-10} to 1×10^{-7} A.

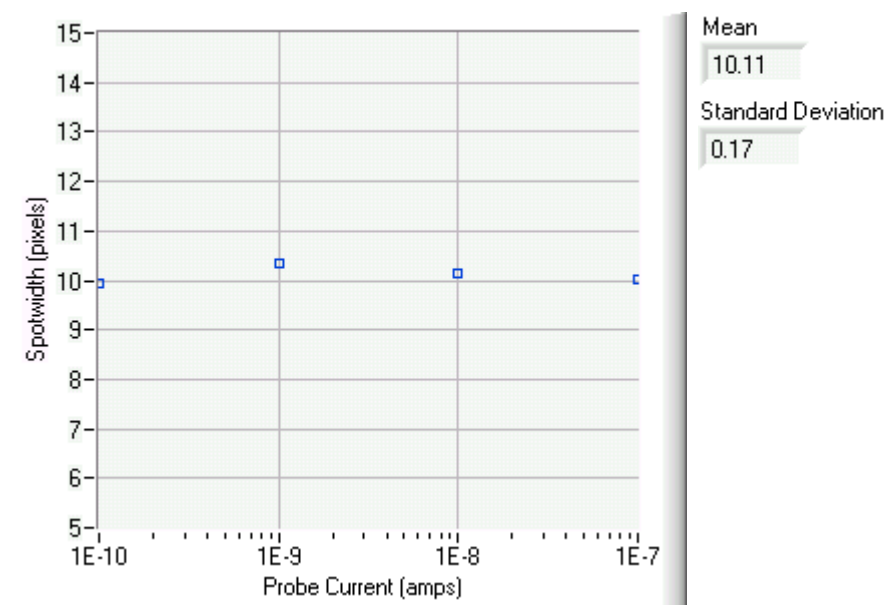


FIGURE 11. Bulk GaAs,
Spotwidth as a Function of Probe Current.

2. Epitaxial AlGaAs

Measurements were made on a 1 μm n-type AlGaAs epitaxial sample without applying any external bias in order to image the spotwidth under conditions of diffusive transport on a thin sample. This sample differs from the previous sample in that it can be approximated as 2D. It was grown on semi-insulating GaAs which has weak luminescence. Figure 12 illustrates the difference in excitation volume for a 2D and 3D sample. The figure illustrates that diffusion length should be able to be measured without luminescence from the area below. The first set of measurements made was the spotwidth as a function of accelerating voltage. Measurements were taken with the probe current at 1×10^{-8} A. It was found that the spotwidth increases as the accelerating voltage increases, as was expected. For example, at 10 kV the spotwidth was 3.32 pixels while at 20 kV the spotwidth was found to be 3.94 pixels. This increase in spotwidth as a function of accelerating voltage has been measured in a number of thin and thick samples.

Next, measurements were taken of the spotwidth while varying the probe current. The accelerating voltage was held constant at 20 kV. Shown in Figure 13 are the spots for various probe currents. It can be seen that as the probe current increases the spotwidth increases. Shown in Figure 14 is a graph of the spotwidth as a function of probe current. This increase in spotwidth is most likely due to being approximately in the 2D limit, i.e., the layer is thinner than the excitation volume. The increase in the electron beam from the probe current increase is small. This series of experiments was repeated with an accelerating voltage of 10 kV and the same trend was observed. The spotwidths as a function of probe current are compared for 1 μm AlGaAs and Bulk GaAs in Figure 15. It is seen from this figure that the spotwidth changes only for the thin approximately 2D sample.

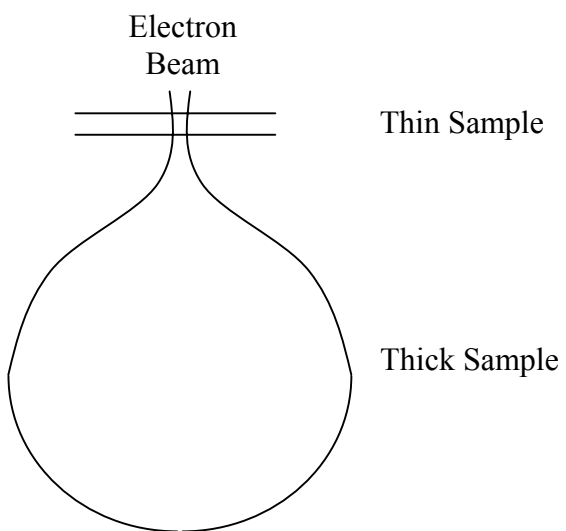


FIGURE 12. Excitation Volume, 2D and 3D Sample.

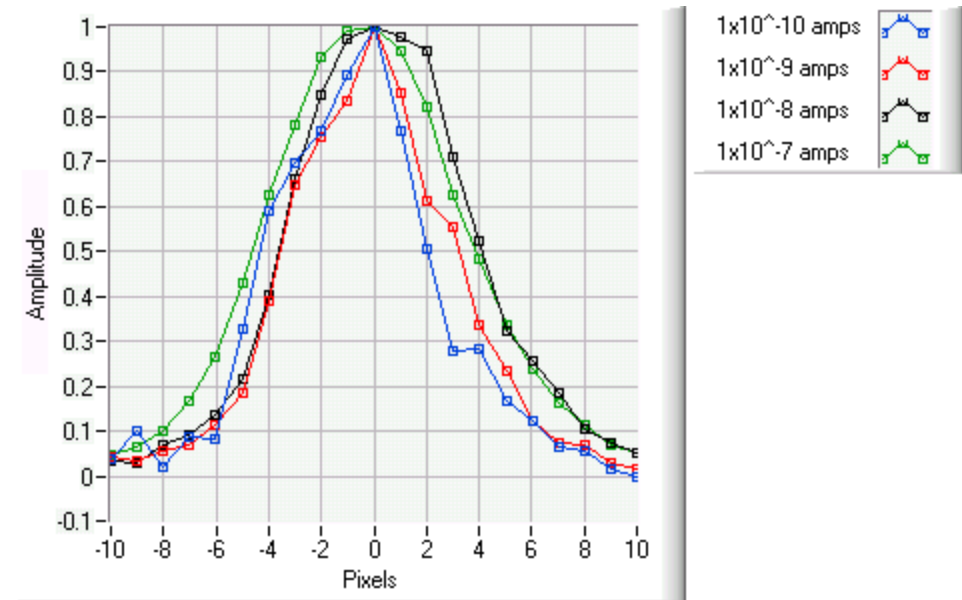


FIGURE 13. $1\ \mu\text{m}$ AlGaAs,
Luminescent Spot for Probe Currents 1×10^{-10} to 1×10^{-7} A.

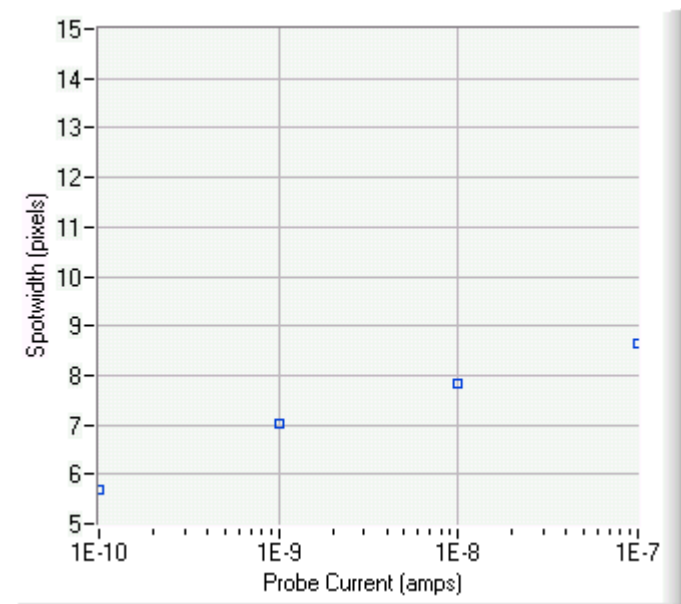
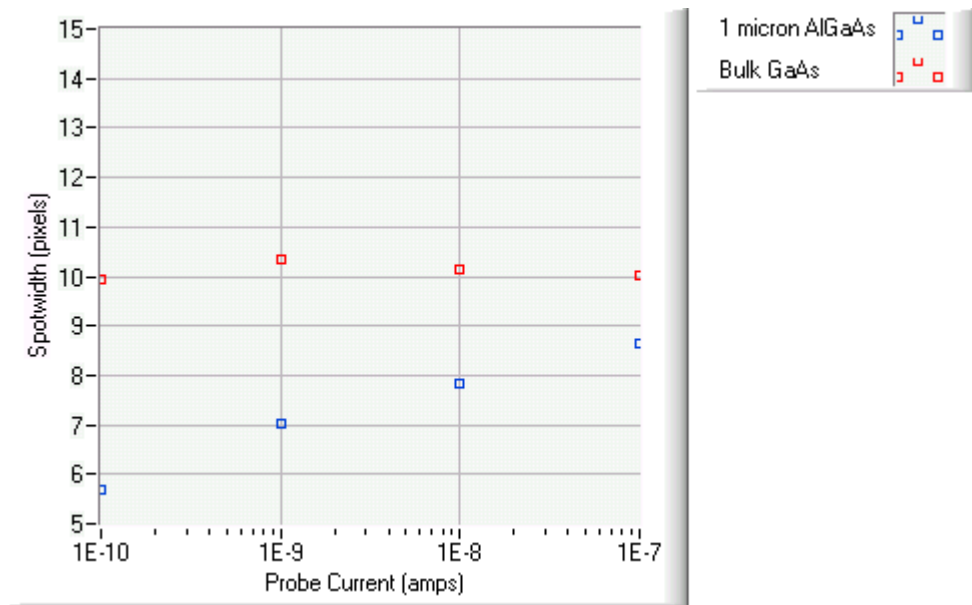
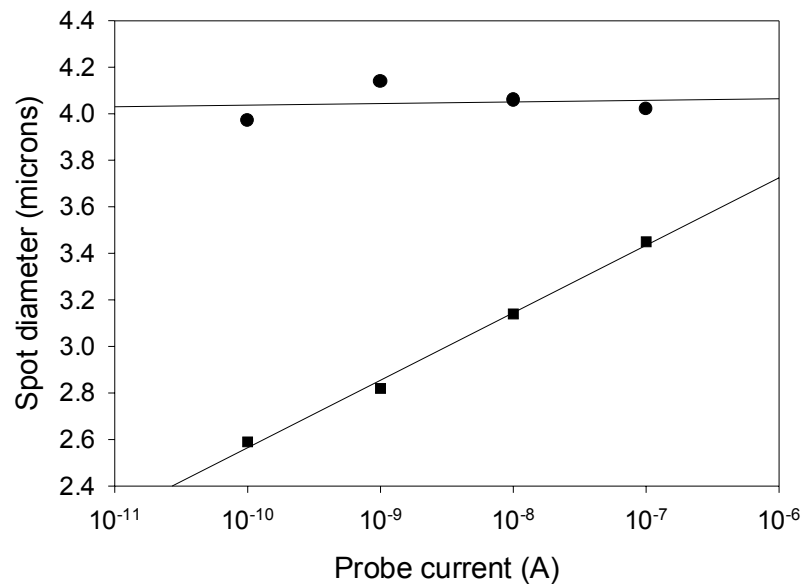


FIGURE 14. $1\ \mu\text{m}$ AlGaAs,
Spotwidth as a Function of Probe Current.



(a) Raw data.



(b) Fitted data.

FIGURE 15. 1 μm AlGaAs and Bulk GaAs, Spotwidth as a Function of Probe Current (■ 1 μm AlGaAs, ● Bulk GaAs).

3. GaAs/GaNAs Quantum Well

Since the AlGaAs data showed that the spotwidth varied as a function of probe current for thin samples in the 2D approximation, this suggests the spotwidth is a function of diffusive parameters rather than generation conditions for 2D samples. Thus, a series of samples were required in which only diffusion lengths would be expected to vary, with all other parameters such as material layer thickness and growth techniques held constant.

The next samples measured were GaAs/GaNAs quantum wells (QWs) obtained from Stanford University. There were three samples measured and all three had the following layered structure.

500 Å	GaAs
200 Å	GaNAs
3,000 Å	GaAs

The main difference between the samples was the substrate growth temperatures. This was of interest to this experiment since often higher growth temperatures lead to longer diffusion lengths and better quality material. Other growth conditions were the same. All of the samples have been rapid thermal annealed at 820 °C for 60 sec. This was done to improve optical quality. Listed below are the growth temperatures for the three samples.

n554a
Substrate Temperature = 475 °C

n546
Substrate Temperature = 525 °C

n553
Substrate Temperature = 575 °C

The first surface layer of 500 Å most likely does not luminesce much as generally the first tenth of a micron is usually dominated by surface recombination. Likewise, the bulk substrate underneath the first three layers should not luminesce much either since it is semi-insulating GaAs. Thus, the two layers that should luminesce most are the 200 Å GaNAs layer and the 3,000 Å GaAs buffer.

The bandgap of GaAs is 1.42 eV corresponding to a wavelength of 870 nm, while for GaNAs PL measurements showed the peak at 1,070 nm wavelength corresponding to a bandgap of approximately 1.16 eV (measurements taken by Stanford). Due to the

differences in the bandgaps of the layers, it is possible to use a filter so that only one of the two would be detected by the CCD camera at a given time. Measurements were taken panchromatic (without using a filter), with a 950 nm long pass filter (allowing light from the GaNAs layer through, while filtering out light from the GaAs layer), and with a 950 nm short pass filter (allowing light from the GaAs layer through, while filtering out light from the GaNAs layer).

a. Panchromatic

Shown in Figures 16 and 17 are the spots measured from the three samples with a probe current of 1×10^{-7} A. Since this was measured without a filter, light from both the GaAs and GaNAs layers was detected. It is seen that samples n544a and n553 have spotwidths approximately the same. The spotwidth of sample n546 is the largest. Figures 18, 19, and 20 show the three different samples spotwidths taken at three different locations on each sample for two different probe currents (3×10^{-8} and 1×10^{-7} A) to check for reproducibility. It is seen that the standard deviations are small indicating the measurements from the three different locations are about the same. The data shows that even when the same probe current is used, sample n546 has a spotwidth that is larger than that of samples n554a and n553 indicating differences in diffusive behavior. The general trend does not show correlation between larger spotwidth and higher growth temperatures (possible longer diffusion lengths), but since this data did not use a filter the spotwidth was a function of light from both the GaAs and GaNAs layers. In order to isolate illumination from the GaAs and GaNAs layers, filters were used.

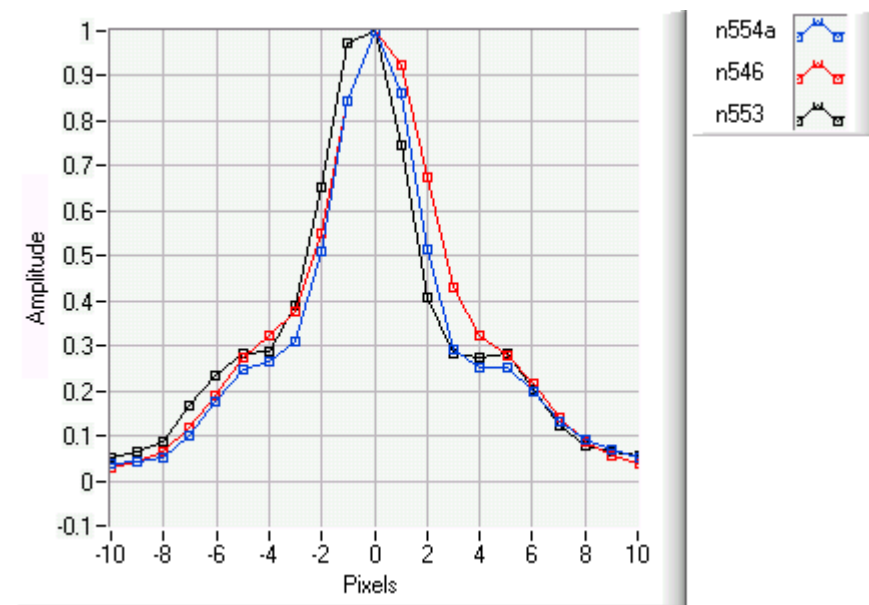


FIGURE 16. GaAs/GaNAs, Panchromatic, Raw Data, Luminescent Spot for Probe Current 1×10^{-7} A.

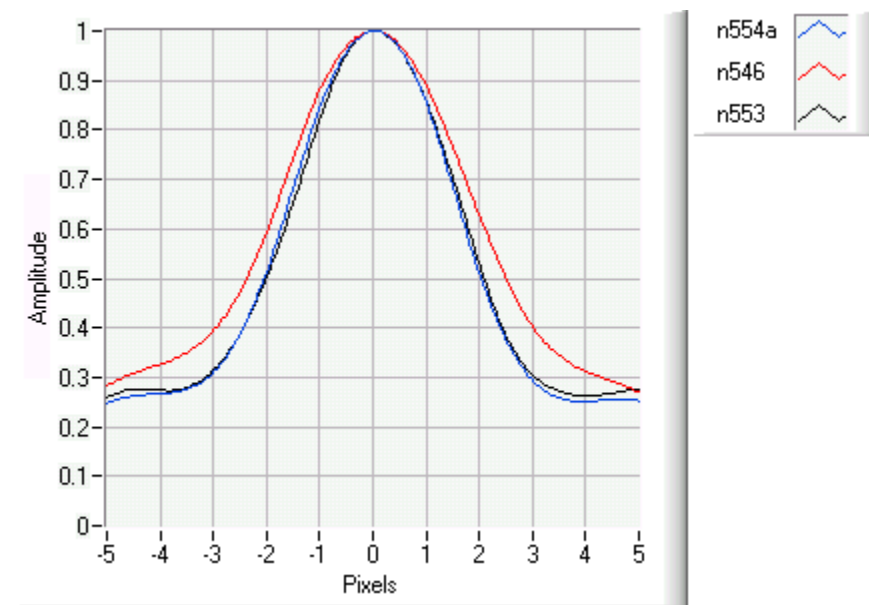


FIGURE 17. GaAs/GaNAs, Panchromatic, Spline Data, Luminescent Spot for Probe Current 1×10^{-7} A.

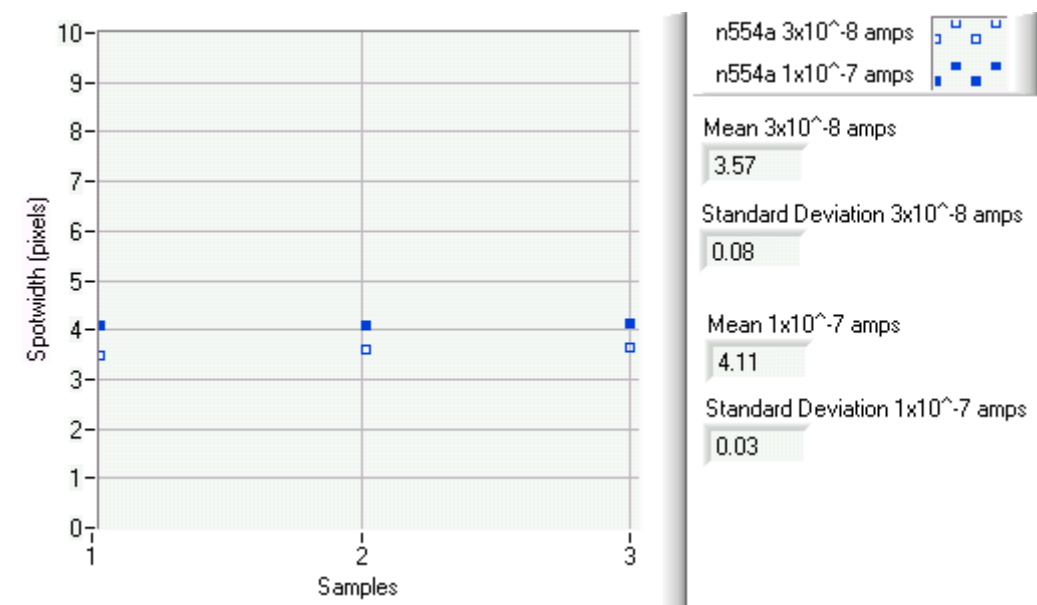


FIGURE 18. GaAs/GaNAs, Sample n554a, Panchromatic, Spotwidth vs Spatial Samples.

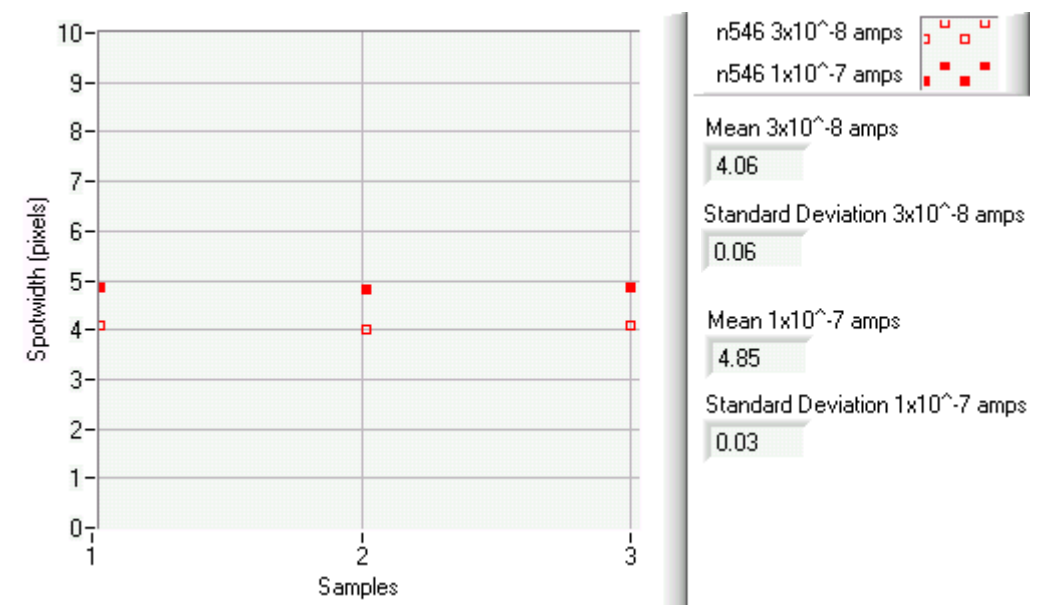


FIGURE 19. GaAs/GaNAs, Sample n546, Panchromatic, Spotwidth vs Spatial Samples.

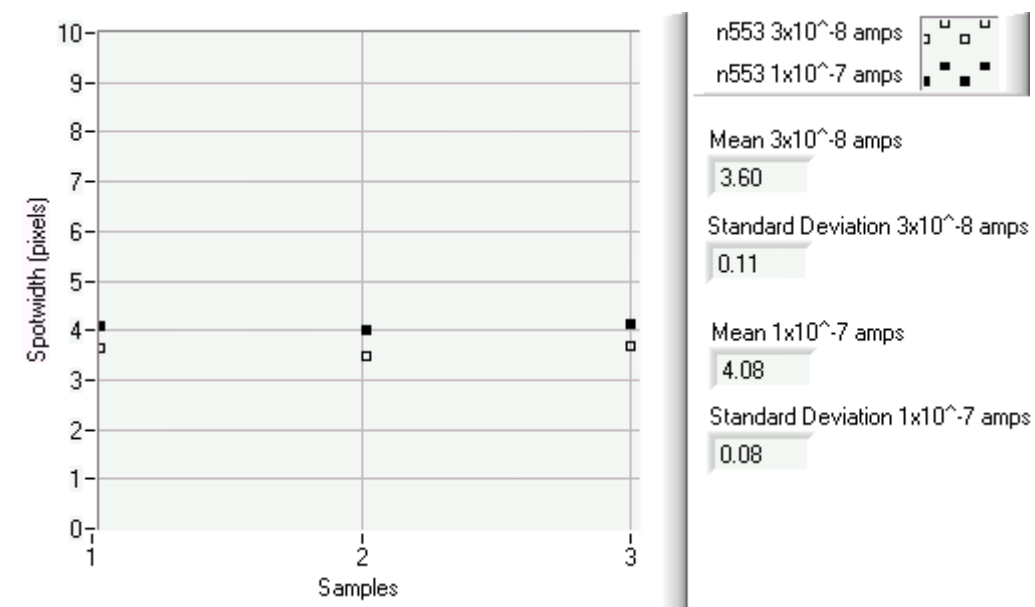


FIGURE 20. GaAs/GaNAs, Sample n553, Panchromatic, Spotwidth vs Spatial Samples.

b. 950 nm Long Pass Filter, GaNAs Layer Luminescence

In order to isolate illumination from the GaNAs layer, a 950 nm long pass filter (LPF) was used. Shown in Figures 21 and 22 are the spots measured from the three samples with a probe current of 1×10^{-7} A. Since this was measured with a 950 nm LPF, only light from the GaNAs layer was detected. It is seen that the spotwidth of sample n546 is the smallest, while the spotwidth of sample n554a is the next largest, and the spotwidth of sample n553 is the largest of the three samples. Figures 23, 24, and 25 show the three different samples spotwidths taken at three different locations on each sample for two different probe currents (3×10^{-8} and 1×10^{-7} A). It is seen that the standard deviations are relatively large indicating differences in the measurements from the three different locations. The data shows that when the same probe current is used, differences in the spotwidths were measured. The general trend does not show correlation between larger spotwidth and higher growth temperatures (possible longer diffusion lengths). However, since the GaNAs process is not believed to be as good as that for GaAs, these results may not be that surprising in that higher growth temperatures may not lead to longer diffusion lengths in the GaNAs layer and there may be more variation. This may be seen from the relatively large deviations in the data. For example, sample n553 showed a standard deviation as high as 0.27 pixels for a probe current of 3×10^{-8} A. This may suggest spatial non-uniformity, which has been previously reported for MBE growth GaNAs.

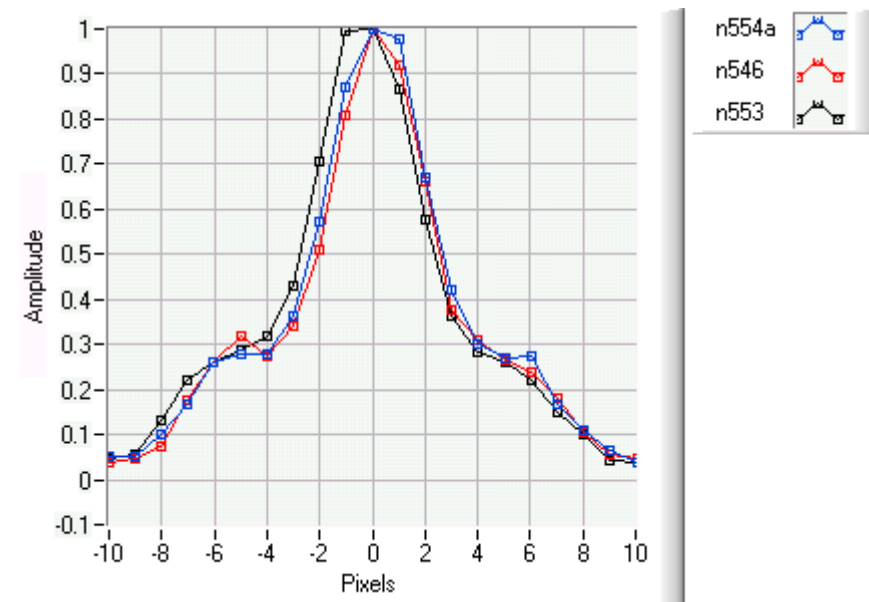


FIGURE 21. GaAs/GaNAs, LPF GaNAs Luminescence, Raw Data, Luminescent Spot for Probe Current 1×10^{-7} A.

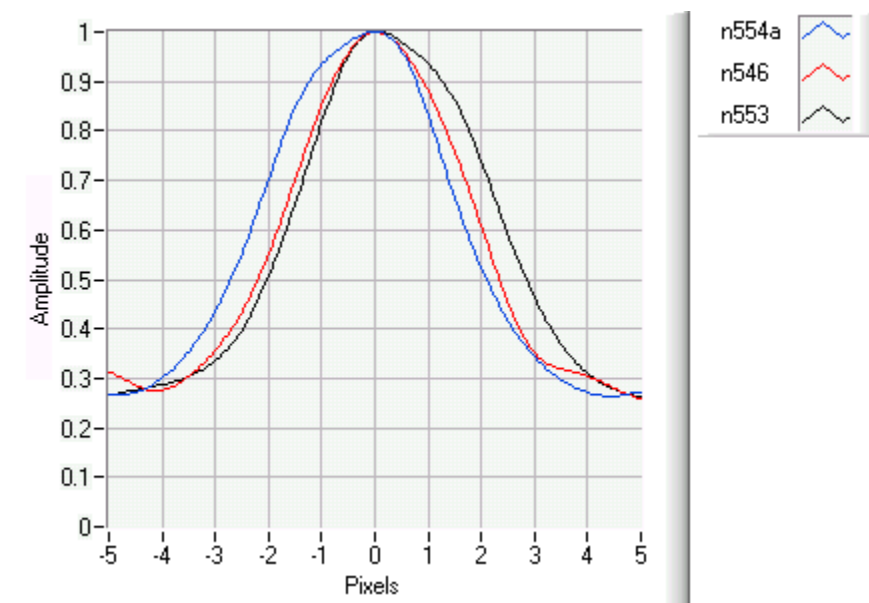


FIGURE 22. GaAs/GaNAs, LPF GaNAs Luminescence, Spline Data, Luminescent Spot for Probe Current 1×10^{-7} A.

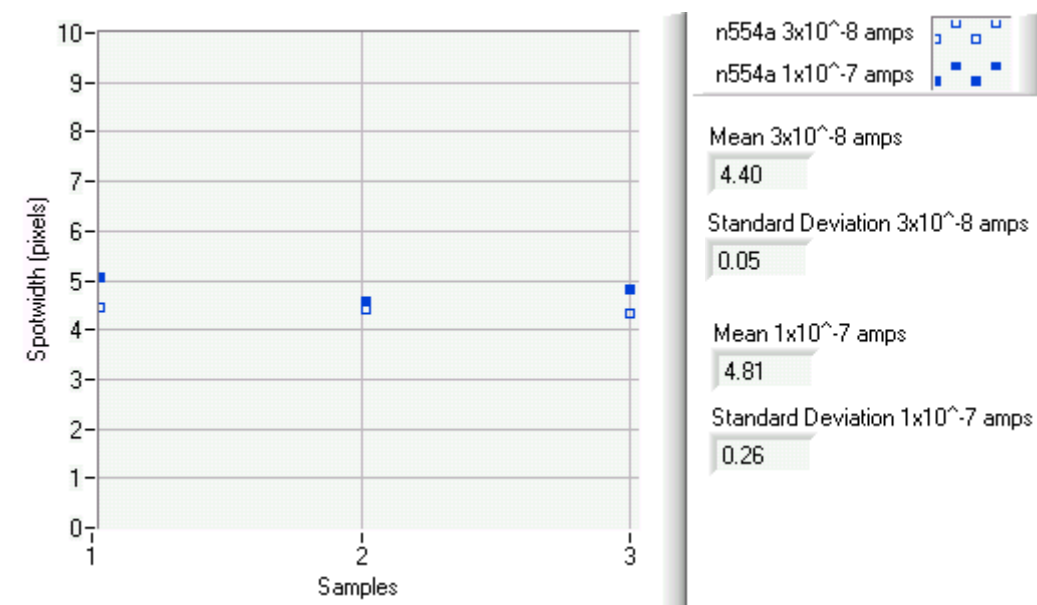


FIGURE 23. GaAs/GaNAs, Sample n554a, LPF GaNAs Luminescence, Spotwidth vs Spatial Samples.

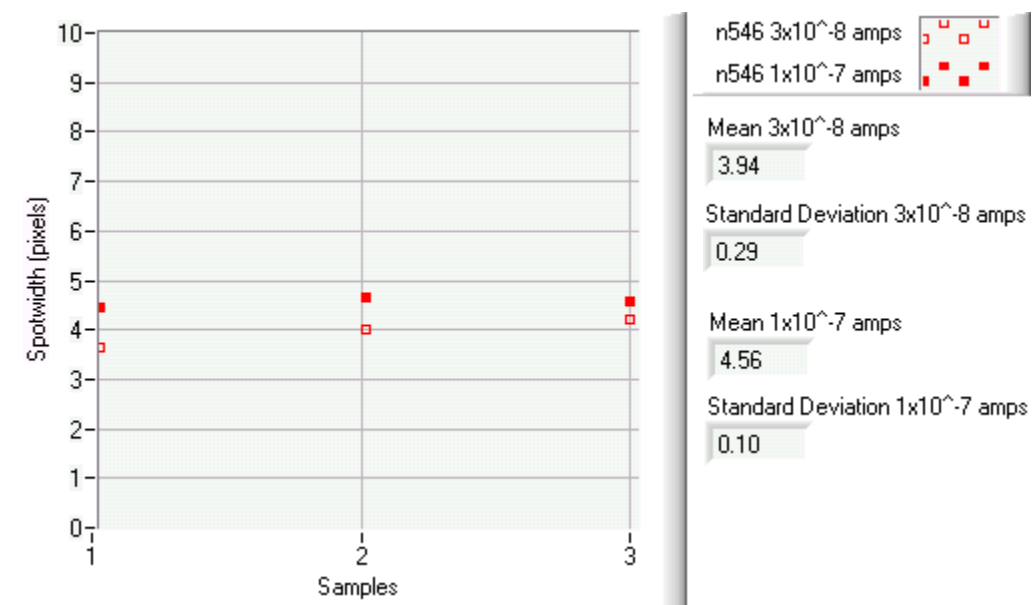


FIGURE 24. GaAs/GaNAs, Sample n546, LPF GaNAs Luminescence, Spotwidth vs Spatial Samples.

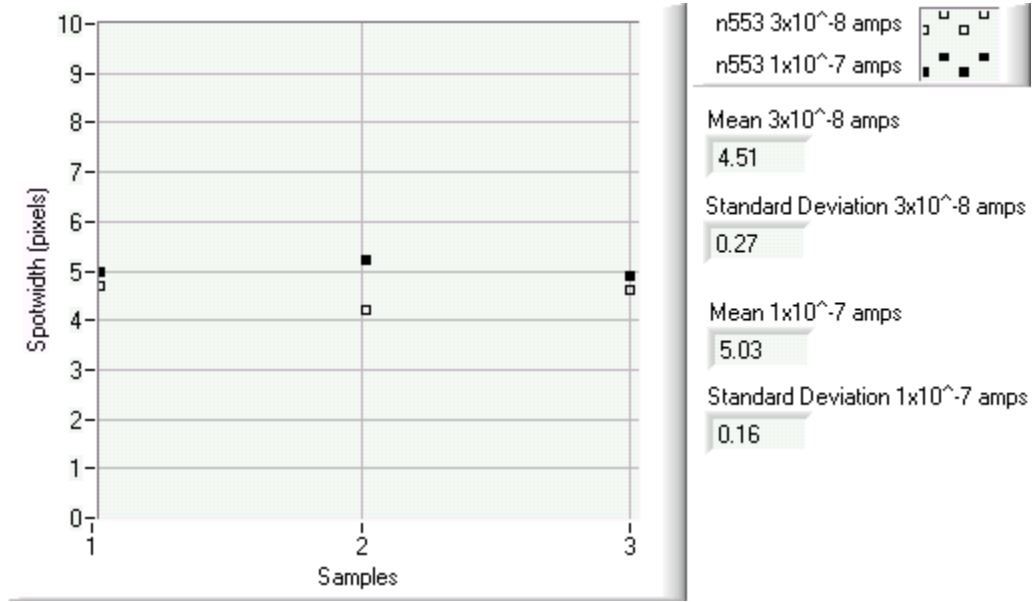


FIGURE 25. GaAs/GaNAs, Sample n553, LPF GaNAs Luminescence, Spotwidth vs Spatial Samples.

c. 950 nm Short Pass Filter, GaAs Layer Luminescence

The next set of measurements was done with a 950 nm short pass filter (SPF). This would allow the light from the GaAs layer through while filtering out the light from the GaNAs layer. Shown in Figures 26 and 27 are the spots measured from the three samples with a probe current of 1×10^{-7} A. It is seen that the spotwidth of sample n554a is the smallest, while the spotwidth of sample n546 is the next largest, and the spotwidth of sample n553 is the largest of the three samples. The process of growing the GaAs layer is believed to be much better than for the GaNAs layer. Generally speaking, the minority carrier lifetime and therefore the diffusion lengths of GaAs will increase with increasing growth temperature. Thus, the trend is as expected since the spotwidth is increasing as a function of growth temperature (and more than likely the diffusion length) for the GaAs layer. This indicates that the spotwidth for a sample that can be approximated as 2D may be a function of the diffusion length.

Figures 28, 29, and 30 show data taken at three different locations on each sample for two different probe currents (3×10^{-8} and 1×10^{-7} A). It was found that for the probe current of 3×10^{-8} A sample n544a had a mean spotwidth of 3.36 pixels with a

standard deviation of 0.03 pixels, and for a probe current of 1×10^{-7} A had a mean spotwidth of 3.74 pixels with a standard deviation of 0.00 pixels. It was found that for the probe current of 3×10^{-8} A sample n546 had a mean spotwidth of 3.41 pixels with a standard deviation of 0.03 pixels, and for a probe current of 1×10^{-7} A had a mean spotwidth of 3.86 pixels with a standard deviation of 0.16 pixels. It was found that for the probe current of 3×10^{-8} A sample n553 had a mean spotwidth of 3.77 pixels with a standard deviation of 0.11 pixels, and for a probe current of 1×10^{-7} A had a mean spotwidth of 4.37 pixels with a standard deviation of 0.21 pixels.

It should be noted that there was some deviations in the data. There were two locations (two samples) that did not show the spotwidth increasing as a function of growth temperature, though the average did show an increase as a function of growth temperature. And there was never a case where the trend was backwards, i.e., the spotwidth always increased (or remained the same in two of the measurements) as a function of growth temperature. This data does indicate that there is potential to extract diffusion parameters from the spotwidth on 2D samples with a technique that is sensitive to both small changes in diffusion length as well as spatial variations. In the next section, a numerical model will be applied to relate the variations in spotwidth to a quantitative measure of diffusion lengths.

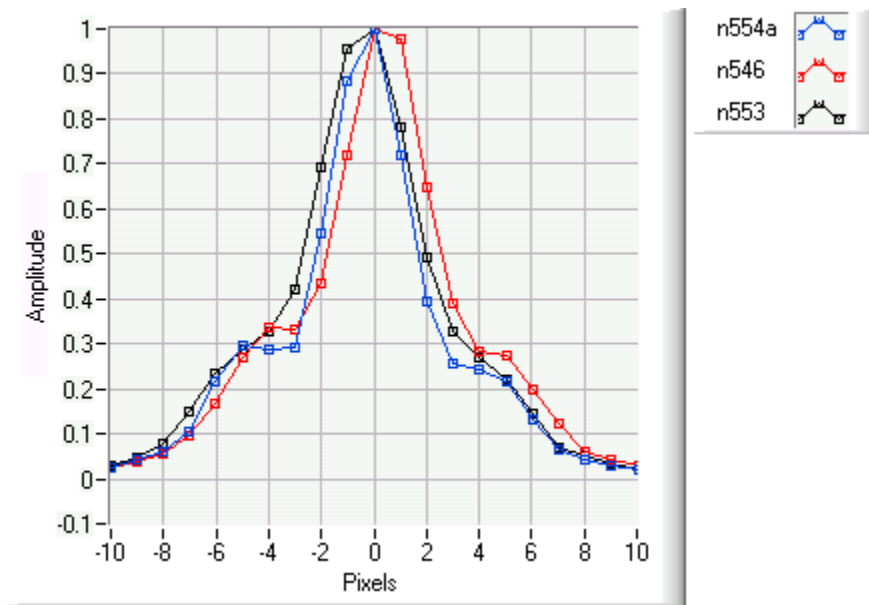


FIGURE 26. GaAs/GaNAs, SPF GaAs Luminescence, Raw Data, Luminescent Spot for Probe Current 1×10^{-7} A.

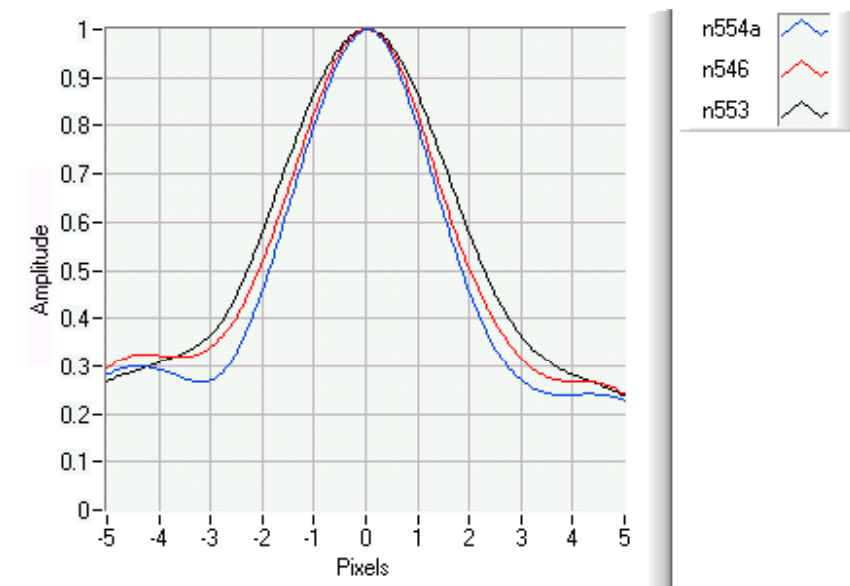


FIGURE 27. GaAs/GaNAs, SPF GaAs Luminescence, Spline Data, Luminescent Spot for Probe Current 1×10^{-7} A.

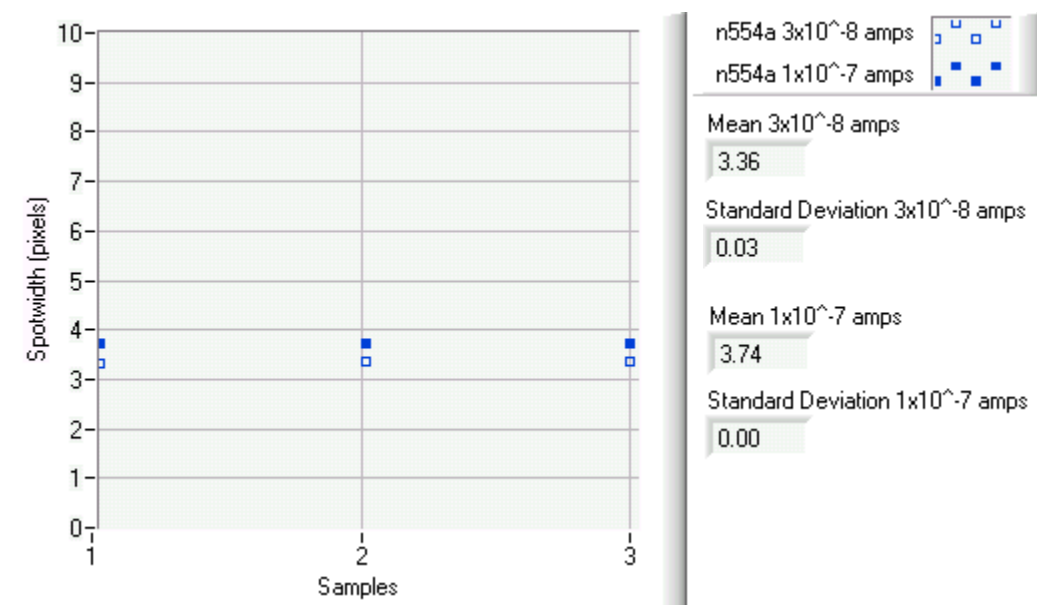


FIGURE 28. GaAs/GaNAs, Sample n554a, SPF GaAs Luminescence, Spotwidth vs Spatial Samples.

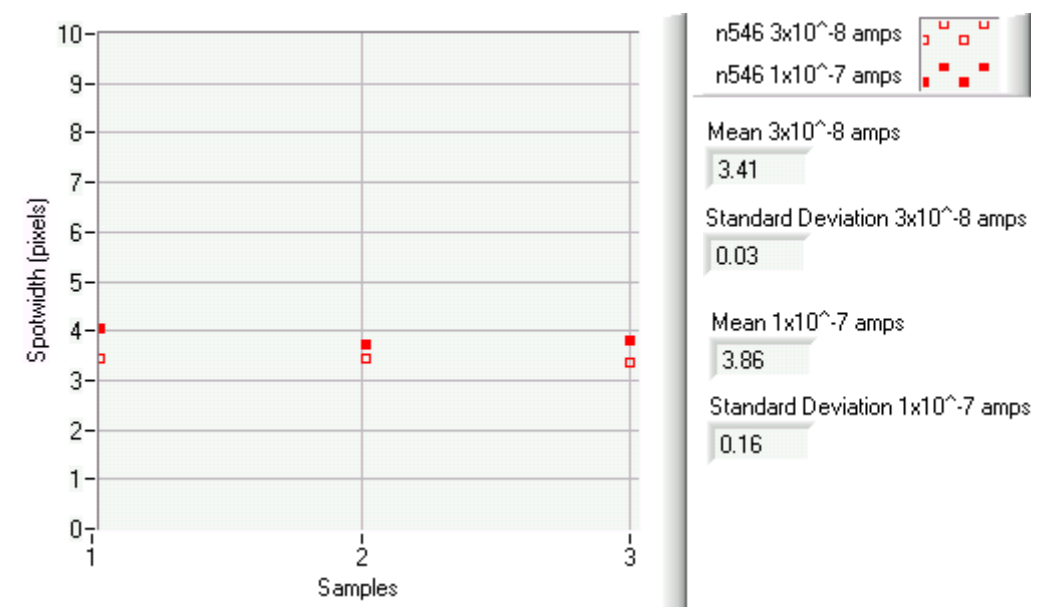


FIGURE 29. GaAs/GaNAs, Sample n546, SPF GaAs Luminescence, Spotwidth vs Spatial Samples.

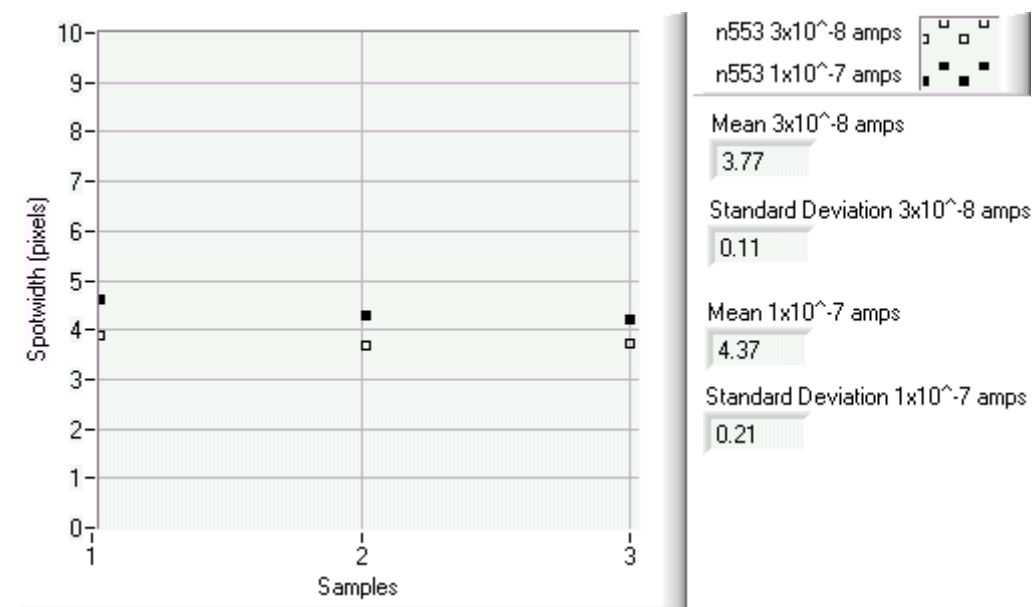


FIGURE 30. GaAs/GaNAs, Sample n553, SPF GaAs Luminescence, Spotwidth vs Spatial Samples.

D. COMPARISON TO COMPUTER MODEL

A computer model to simulate diffusion and drift of minority carriers and their recombination was developed [1]. The model includes diffusion and a 1D applied electric field for the bias. The minority carrier distribution is given by

$$\varpi = \frac{n^2}{2\pi^2(L_{diffusion})^2} \int_{y-\frac{1}{2n}}^{y+\frac{1}{2n}} \int_{x-\frac{1}{2n}}^{x+\frac{1}{2n}} e^{\frac{(L_{drift})\xi}{2(L_{diffusion})^2}} K_0 \left(\frac{\sqrt{(L_{drift})^2 + 4(L_{diffusion})^2}}{2(L_{diffusion})^2} r \right) d\xi d\eta \quad (14)$$

where K_0 is a zero order modified Bessel function of the second kind and $r = (\xi^2 + \eta^2)^{1/2}$. The model was run for the case with a bias of 550 V/cm and $L_{diffusion} = 4.3 \mu\text{m}$. As with the earlier experimentally measured data, the final image was produced by subtraction of images with and without the applied electric field. Shown in Figure 31a is the computer model generated simulation of transport for this case [13]. The image size is $60 \times 180 \mu\text{m}$. As a comparison, shown in Figure 31b is the measured charge transport recombination in epitaxial layers of n-type GaAs (329SI) with $E = 550 \text{ V/cm}$. It can be seen that the model produces results in close agreement with that measured.

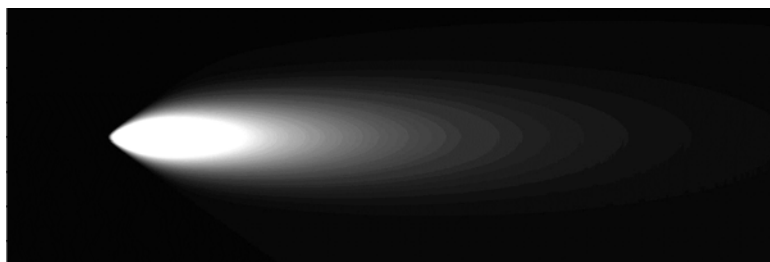
The model was also run with the bias set to zero in order to model diffusive behavior. The model currently exists in two forms, one that assumes a point source (Dirac delta function) and another that allows for a finite generation region. The electron beam incident on the surface of the sample is approximated to be square (rather than circular). Setting the length of the sides of the square to $2 \mu\text{m}$ (which is a reasonable estimate), spotwidths were calculated while varying the mobility lifetime product ($\mu\tau$). Shown in Figure 32 are the computer modeled spots for various mobility lifetime products. The mobility lifetime products and corresponding spotwidths found were

$\mu\tau \text{ (cm}^2\text{/V)}$	Spotwidth (pixels)
1.60×10^{-6}	3.74
1.80×10^{-6}	3.87
3.48×10^{-6}	4.34

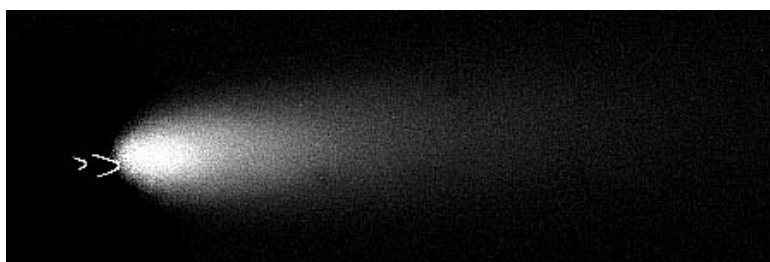
These spotwidths are approximately the same as the averages calculated for the GaAs/GaNAs samples with the SPF (such that luminescence is from the GaAs layer) and a probe current of $1 \times 10^{-7} \text{ A}$. Comparison of Figure 32 to Figure 27 shows that the modeled spotwidths are very close to the measured spotwidths. It is noted that there are

some slight differences in the spot shape, including background and thermal noise. These may be attributed to the square approximation and other approximations. Further improvements to the modeled are planned. It is seen from Figure 27 that the difference in spotwidth from samples n554a and n546 looks greater than that modeled, however, this is because Figure 27 is showing just one of the sampled locations. The means (from the three locations) shown in Figures 28, 29, and 30 are approximately the same as that predicted by the model. If the mobility is assumed to be $400 \text{ cm}^2/(\text{Vs})$, the corresponding lifetimes for the three mobility lifetime products (in order of increasing product) would be 4.0, 4.5, and 8.7 nsec respectively. Thus, the initial results suggest that the technique, in its current form, may be sensitive to changes of a factor of approximately 0.5 nsec in lifetime.

One potential use of the transport imaging technique would be to measure local diffusion lengths. Since the model has been shown to be in close agreement with measured results, it could possibly be used to match the spotwidth of a measured sample and thus the mobility lifetime product for the sample could be estimated. The ideal case would be to take measurements on samples with known diffusion lengths. This was unavailable at the time these measurements were taken and is something that is planned for future experimental measurements. The advantage to using this approach, as opposed to conventional techniques discussed earlier, is that the sample does not have to have contacts. Contact-less diffusion measurements could provide a cost savings since the expense of contact processing on the sample would not be there. Likewise for the applied bias case, diffusion parameters could also potentially be estimated by matching the drift in the measured images to that predicted by computer modeling. Knowing the applied electric field and the mobility lifetime product would yield an estimate for the drift length.



(a) Computer model.



(b) Measured data.

FIGURE 31. Computer Modeled and Measured Charge Motion Under Applied Bias, Subtracted.

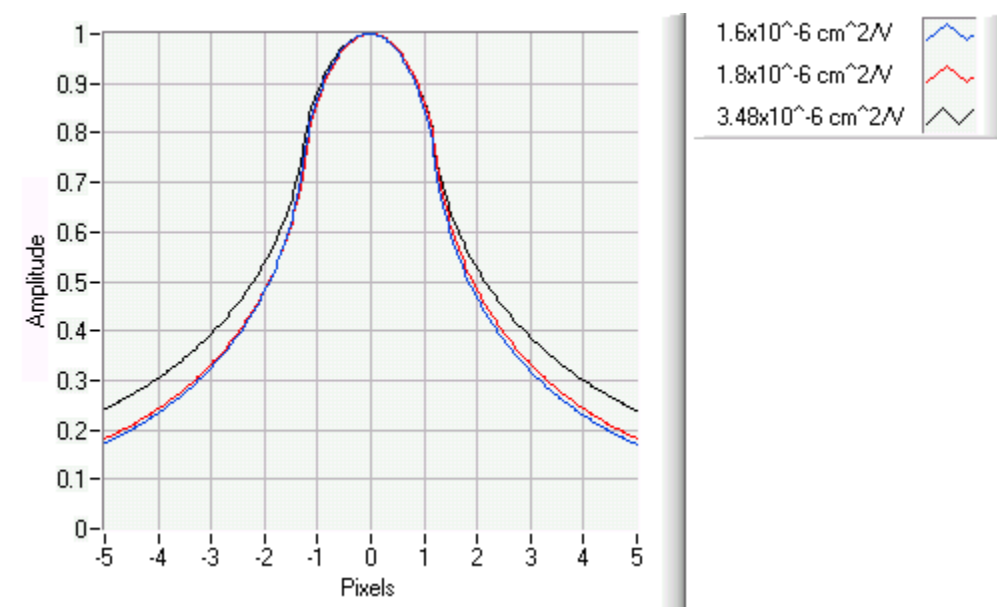


FIGURE 32. Computer Modeled Spot for Mobility Lifetime Products 1.6×10^{-6} , 1.8×10^{-6} , and $3.48 \times 10^{-6} \text{ cm}^2/\text{V}$.

IV. CONCLUSIONS

Imaging charge carrier motion in a number of semiconductor samples has been demonstrated using the charge transport imaging technique both with and without the application of external bias. Measured results were compared for both the biased and unbiased cases to that predicted by computer modeling and the simulated results were very close to that measured. It was found that for the unbiased case, spotwidths did not change as a function of probe current on bulk 3D samples. However, the spotwidths were found to change for thin samples that could be approximated as 2D as the probe current was varied. Measurements were made using a SPF on GaAs/GaNAs QW samples so that most of the luminescence would be from the GaAs layer. The difference between the samples was that the growth temperatures were different. It was found that the spotwidths increased as the growth temperature increased. Since the lifetime often increases as growth temperature increases, this indicated that the spotwidth may be a function of diffusive parameters for 2D samples.

A close examination of the spotwidth (from 2D intensity graphs) reveals that the spot is not perfectly circular. This possibly could be a result of the electron beam not being perfectly circular (remembering the current system has sub-micron scale resolution). Because of this, it may be advantageous to use the area of the spot rather than 1D cuts through the spot [10]. Another area of improvement would be to replace the optics to get better resolution. This would allow more accurate estimates of the spotwidth. This is something that is planned in the future.

While it has been shown that the computer modeling and actual measured data are in close agreement, the feasibility of contact-less diffusion measurements does require some additional practical considerations. As discussed earlier, the ideal case would be to get samples with known mobility and lifetimes to be used as a standard. Such samples may be attainable to the degree required from the solar cell community, as knowledge of these parameters is critical for their design and optimization.

Another possible use of the transport imaging technique using an applied bias is for detecting defects in samples. Current interest particularly from the solar cell

community is for doing just that. Since this technique allows for sub-micron scale spatial resolution, defects could potentially be mapped to a high degree of accuracy. Another potential application is for mapping electric fields present between contacts due to the space charge layer. While electric fields have been modeled using different techniques (some neglecting the space charge layer), this could provide a means of measuring the fields with good resolution. Both of these topics remain active areas of ongoing research.

LIST OF REFERENCES

1. Haegel, N.M., Fabbri, J.D., and Coleman, M.P., "Direct Transport Imaging in Planar Structures," *Appl. Phys. Letters* **84**, 1329 (2004).
2. Karunasiri, G., "Semiconductor Device Physics," Course Notes, Naval Postgraduate School, Monterey, CA, 2004.
3. Kasap, S.O., *Principles of Electronic Materials and Devices*, 4th Edition, McGraw-Hill, New York, NY, 2002.
4. Sze, S. *Physics of Semiconductor Devices*, 2nd Edition, John Wiley & Sons, New York, NY, 1981.
5. Stevenson, D.J. and Keyes, R.J., "Measurement of Carrier Lifetime in Germanium and Silicon," *J. Appl. Phys.* **26**, 190 (1955).
6. Haynes, J.R., and Shockley, W., "The Mobility and Life of Injected Holes and Electrons in Germanium," *Phy. Rev.* **81**, 835 (1951).
7. Yacobi, B.G. and Holt, D.B., *Cathodoluminescence Microscopy of Inorganic Solids*, Plenum Press, New York, NY, 1990.
8. Kanaya, K., and Okayama, S., "Penetration and Energy-Loss Theory of Electrons in Solid Targets," *J. Phys. D: Appl. Phys.* **5**, 43 (1972).
9. Everhart, T.E., and Hoff, P.H., "Determination of Kilovolt Electron Energy Dissipation vs Penetration Distance in Solid Materials," *J. Appl. Phys.* **42**, 5837 (1971).
10. Hoang, V.D., "Charge Transport Study of InGaAs QWIPS," Master's Thesis, Naval Postgraduate School, Monterey, CA, June 2004.
11. Donolato, C., "On the Theory of SEM Charge-Collection Imaging of Localized Defects in Semiconductors," *Optik* **52**, 19 (1978).
12. LabVIEW Function and VI Reference Manual, National Instruments, Austin, TX, 1998.
13. Haegel, N.M., Hoang, V.D., and Freeman, W., "Imaging Transport: Monitoring the Motion of Charge Through the Detection of Light," *ICPS*, July 2004.

THIS PAGE INTENTIONALLY LEFT BLANK

INITIAL DISTRIBUTION LIST

1. Defense Technical Information Center
Fort Belvoir, VA
2. Dudley Knox Library
Naval Postgraduate School
Monterey, CA
3. Professor James H. Luscombe, Chairman, Department of Physics
Naval Postgraduate School
Monterey, CA
4. Professor Nancy M. Haegel
Naval Postgraduate School
Monterey, CA
5. Will Freeman
NAWCWD
China Lake, CA